SUPPORTING INFORMATION

Organic solar powered greenhouse performance optimization and global economic opportunity

Eshwar Ravishankar,[a] Ronald E. Booth,[a] Joseph A. Hollingsworth,[b] Harald Ade,[c] Heike Sederoff,[d] Joseph F. DeCarolis [b] and Brendan T. O'Connor [a*]

a Department of Mechanical and Aerospace Engineering, and Organic and Carbon Electronics Laboratories (ORaCEL), NC State University, Raleigh, NC, 27695, USA.

b Department of Civil, Construction, and Environmental Engineering, NC State University, Raleigh, NC, 27695, USA.

c Department of Physics, and ORaCEL, NC State University, Raleigh, NC, 27695, USA.

d Department of Plant and Microbial Biology, NC State University, Raleigh, NC, 27607, USA.

* Correspondence and Lead Contact: btoconno@ncsu.edu

1. Description of lettuce growth model

The plant growth model considered here is made of sub-models representing each aspect of biomass production such as total leaf area expansion, impact of environmental parameters that include sunlight, temperature and CO_2, photosynthesis, and associated growth and respiration losses required to maintain cells, their biostructure and ionic gradients. The flowchart depicting the relation between these parameters leading to biomass production is shown in **Figure 1** and the underlying mathematical equations and parameters involved are highlighted here.

1.1. Determining orientation and light interception by leaves

Sunlight absorbed by the plants depends on the orientation of the leaves. This is modelled based on the assumption that the plant canopy will be considered as consisting of leaves at different depths as shown in **Figure S1**. Each leaf is capable of absorbing and scattering light and leaves can have various configurations.[1] Each configuration has a certain absorption and scattering defined by a plant effective extinction coefficient (PEEC). PEEC is defined as the ratio of area of leaf to the area of the shadow cast by incident sunlight.[2] This is a measure of interception of light by a leaf. Area of shadow cast changes depending on the angle of incidence of the sunlight and hence, the value of PEEC can vary based on leaf configuration. A horizontal leaf configuration has a PEEC equal to 1 which denotes the area of leaf being equal to area of shade. Similarly, values greater than or less than 1 denotes a leaf area greater or less than area of shade, respectively. PEEC values differ between diffuse and direct solar radiation. While the direct solar radiation comes only in one direction at a particular instant, diffuse radiation is assumed to be uniformly distributed across all directions as depicted in **Figure S1**. Here, for direct solar radiation, we assume a horizontal leaf configuration with the leaves capable of scattering part of the light. Extinction coefficient for direct radiation assuming scattering is derived considering two layers of the plant canopy with each layer consisting of leaves in a horizontal configuration.[1] Light flux leaving layer n and n+1 and travelling in the downward direction is given by,

$$\Phi_{d,n+1} = \Phi_{d,n}\left((1 - \Delta L) + T_{leaf}\Delta L\right) + \Phi_{u,n+1}\rho_{leaf}\Delta L, \tag{1}$$

$$\Phi_{d,n+1} = \Phi_{u,n+1}\left((1 - \Delta L) + T_{leaf}\Delta L\right) + \Phi_{d,n}\rho_{leaf}\Delta L. \tag{2}$$

where $\Phi_{d,n+1}$ and $\Phi_{d,n}$ denotes light flux travelling through layer n and n+1 respectively in the downward direction, $\Phi_{u,n+1}$ and $\Phi_{u,n}$ denotes light flux travelling through layer n and n+1

2

respectively in the upward direction, ΔL denotes gap between leaves, R and T denote reflectance and transmittance respectively. Solving equation (1) and equation (2) simultaneously, The PPEC for direct radiation assuming scattering is given by,

$$PEEC_{direct} = PEEC_{bl}\sqrt{1 - \sigma}, \tag{3}$$

where $PEEC_{bl}$ is the extinction coefficient of leaves with no scattering and has value of 1, σ is the scattering coefficient which is defined as the sum of reflectance (R) and transmittance (T) of a single healthy leaf.

In the case of diffuse radiation, sunlight is incident on the leaves from all directions in the horizon and each light will be intercepted at a different rate based on the extinction coefficient at that angle of incidence. Here, the leaves are assumed to be distributed in a spherical distribution. Within the spherical configuration, the leaves are randomly oriented and have different PEECs. Overall, the configuration is assigned a PEEC of 0.5.[1] A realistic distribution of sky brightness for diffuse radiation is given by the isotropic light distribution model.[1] It is assumed that diffuse radiation is averaged across three sky zones. These three sky zones are assumed to supply a fraction of 0.178, 0.514 and 0.308 of the diffuse radiation at an angle of incidence of 15°, 45° and 75°, respectively. At each angle of incidence, PEEC for leaf in a spherical configuration is given by,

$$PEEC_{spher,I} = \frac{0.5}{Sin(\beta)}, \tag{4}$$

where β is the angle of incidence of sunlight on the leaf.

Transmitted flux is given by,

$$\Phi_T = \Phi_I((0.178\exp(-1.93L) + (0.514\exp(-0.707L)) + (0.308\exp(-0.518L)), \tag{5}$$

where Φ_T denotes light flux transmitted through a leaf, Φ_I denotes light flux incident on a leaf, L denotes leaf area index. 1.93, 0.707 and 0.518 are PEECs for a leaf in a spherical configuration at angle of incidences 15°, 45° and 75°. From equation (5), PEEC of diffuse radiation accounting for scattering from the leaves,

$$PEEC_{diff} = \frac{-\ln(\frac{-\Phi_{transmitted}}{\Phi_{incident}})}{L}\sqrt{1-\sigma}. \tag{6}$$

1.2. Light absorption by plant canopy

To model light absorption by the plant canopy, we first assume that only 75 % of total incident light on a greenhouse is transmitted because of losses from the greenhouse structure.[3] Total light incident and transmitted into the greenhouse structure is computed using the transfer matrix model

as previously described.[4] The computed PEEC is utilized towards obtaining sunlight absorbed by the plant canopy. Light absorption occurs through by leaves directly exposed to sunlight as well as by leaves that are shaded. Leaves exposed to light receive both direct and diffuse radiation while the shaded leaves receive scattered radiation from leaves exposed to both direct and diffuse radiation.[1] These components are shown in **Figure S1**.

If the absorbed light and associated photosynthesis are to be computed for the complete plant canopy, the absorption per leaf area must be known at several depths in the plant. This is done through a gaussian integration method, where light absorption calculation is computed per leaf area at five different depths in a plant canopy and integrated across the total leaf area index of the plant to determine light absorption and hence photosynthesis.[5] Within the plant canopy, the leaf area is selected symmetrically at different height fractions, with the maximum height being a value of 1. At each height, a weight is added to determine the fraction of total light absorbed at that level. Total absorption per unit leaf area per canopy depth for diffuse sunlight is given by,

$$I_{diff} = PEEC_{diff}I_{diffuse,incident}(1 - \rho_c)\exp(-PEEC_{diff}laic), \tag{7}$$

where, $I_{diffuse,incident}$ is the incident diffuse solar insolation, ρ_c is the plant canopy reflection coefficient defined as total reflection from crop canopy,

$$\rho_c = \frac{1-\sqrt{1-\sigma}}{1+\sqrt{1-\sigma}}, \tag{8}$$

laic is the leaf area index at a particular depth of the plant canopy is given by,

$$laic = x_{gauss}LAI, \tag{9}$$

where x_{gauss} denotes the presence of leaves at different depths of the plant canopy. Similarly, total absorption by leaves per unit leaf area per depth from direct sunlight,

$$I_{direct,total} = PEEC_{direct}I_{direct,incident}(1 - \rho_c)\exp(-PEEC_{direct}laic). \tag{10}$$

Equation (10) computes light absorbed by the plant canopy from incident direct solar radiation. This includes light captured by leaves through direct interception as well as light capture through scattering of light from direct interception. Leaves that directly intercept direct sunlight are per unit leaf area per canopy depth through is computed by the equation,

$$I_{sunlit,direct} = PEEC_{bl}I_{direct,incident}(1 - \sigma)\exp(-PEEC_{bl}laic), \tag{11}$$

Shaded leaves absorb light using both diffuse and scattered sunlight is given by,

$$I_{total,diffuse} = I_{diff} + (I_{direct,total} - I_{sunlit,direct}). \tag{12}$$

1.3. Photosynthesis

Gross rate of photosynthesis is computed by integrating the photosynthetic assimilation of leaves in a plant over the entire canopy. This does not account for CO_2 loss due to respiration. Maximum gross rate of photosynthesis is limited by either light, CO_2 or plant regeneration processes when exposed to both high light and high CO_2. The maximum rate of CO_2 assimilation is limited by three different scenarios,

A. Low light: At sufficient CO_2, with increasing light intensity plants experience a saturation in CO_2 assimilation. This is termed the light saturated maximum rate of photosynthesis (F_{mm}). This parameter changes as a function of both spectra and temperature and is given by,[1,6]

$$F_{mm} = \left(-4.43 + \left(2.11 \text{temp}_{plant}\right) - \left(0.0438 \text{temp}_{plant}^2\right)\right) (\text{spectral-factor}), \tag{13}$$

where temp_{plant} denotes greenhouse plant temperature, spectral-factor denotes parameter impacting maximum rate of photosynthesis as a function of spectra.

B. High light: At high light, there is limitation by CO_2. This is termed CO_2 saturated maximal rate of photosynthesis. The mathematical relation to determine CO_2 saturated rate of photosynthesis is given by,

$$F_{nc} = \frac{C_a - \tau}{r_m + (1.6 r_s) + (1.4 r_{bv})}, \tag{14}$$

where r_m is the mesophyll resistance, r_{bv} is the boundary layer resistance, r_s is the stomatal resistance, C_a denotes CO_2 concentration in ambient environment, τ denotes CO_2 compensation point is given by,

$$\tau = \tau_{25} e^{0.07(T-25)}, \tag{15}$$

where τ_{25} is the CO_2 compensation at 25^0C.

C. High light and high CO_2: At both high light and high CO_2 the rates of the regeneration processes involving other enzymes will become limiting.[1] The assimilation rate will then be particularly sensitive to temperature changes. In this case the maximum rate of photosynthesis is given by the minimum of either light induced- or CO_2 induced-saturation. The saturation photosynthesis rate is denoted by,

$$f_{photmax} = \min(F_{mm}, F_{nc}). \tag{16}$$

The photosynthetic assimilation of shaded and sunlit leaves at a particular depth is given by,

$$f_{phot,inst} = f_{photmax} y, \tag{17}$$

where y is a dimensionless function of absorbed diffuse and direct sunlight by the plants is given by,

$$y = \frac{1+x-\sqrt{(1+x)^2-4x\theta}}{2\theta}, \tag{18}$$

where $x = \frac{c_\epsilon I_{abs,par}}{F_{g,max}}, \tag{19}$

where $I_{abs,par}$ denotes sunlight in the PAR region absorbed by the plants. This equation is applicable to both direct, diffuse and scattered radiation, ϵ, c_ϵ denotes the slope of the linear part of the photosynthesis-light curve is given by,

$$c_\epsilon = \frac{\epsilon(C_a-\tau)}{(C_a+2\tau)}, \tag{20}$$

where C_a denotes greenhouse CO_2 concentration, τ denotes CO_2 compensation point which is the point where the uptake of CO_2 equals the respiratory release of CO_2.

At each considered depth in the plant canopy, the local assimilation rate is given by,

$$f_{phot,local} = frac_{sun}f_{phot,inst,sun} + (1 - frac_{sun})f_{phot,inst,shd}, \tag{21}$$

where $frac_{sun}$ is the fraction of sunlit leaf area is defined by,

$$frac_{sun} = e^{-PEEC_{bl}laic}. \tag{22}$$

Finally, plant canopy gross photosynthetic assimilation rate is given by,

$$f_{phot,gros} = LAI \sum_{i=1}^{5} w_{gauss}(i)FGL(i), \tag{23}$$

where w_{gauss} is the weight associated with assimilation rate at different canopy depths.

1.4. Computing plant dry mass

The plant dry mass module describes the dynamic behavior of the two state variables – non-structural dry weight (X_{nsdw}) and structural dry weight X_{sdw} on a square-meter soil basis.[2] Dry mass does not include water content in the plant.[7]

$$\frac{dX_{nsdw}}{dt} = c_\alpha f_{phot}\Phi_{PSII} - r_{gr}X_{sdw} - f_{resp} - \frac{1-c_\beta}{c_\beta}r_{gr}X_{sdw}, \tag{24}$$

$$\frac{dX_{sdw}}{dt} = r_{gr}X_{sdw}. \tag{25}$$

where X_{nsdw} and X_{sdw} are the dry weight of non-structural and structural material, c_α is the factor converting CO_2 assimilated into CH_2O, c_β is the Respiratory and synthesis losses of non-structural material due to growth, f_{phot} is the rate of CO_2 assimilation through photosynthesis, Φ_{PSII} is the quantum yield of photosystem II (PSII), r_{gr} is the relative growth rate and f_{resp} is the maintenance

respiration loss. The relative growth rate of structural dry matter depends only on the rate at which non-structural material is transformed into structural material. It is assumed that the growth rate obeys the Michaelis Menten equation given by,[2]

$$r_{gr} = c_{gr,max} \frac{X_{nsdw}}{c_Y X_{sdw} + X_{nsdw}} c_{Q10,gr}^{(temp_{plant}-20)/20}, \tag{26}$$

where $c_{gr,max}$ is the saturation growth rate at 20 °C, c_Y denotes parameter that determines the rate of r_{gr}. $C_{Q10,gr}$ denotes Q10 factor for growth which has a value of 1.6. Q10 factor denotes the value by which the relative growth rate changes at different plant temperature. The maintenance respiration of the crop is given by,

$$f_{resp} = \left(c_{resp,sht}(1 - c_\tau)X_{sdw} + c_{resp,rt}c_\tau X_{sdw}\right)c_{Q10,resp}^{(T-25)/10}, \tag{27}$$

where $c_{resp,sht}$ is the maintenance respiration coefficient for the shoot at 25^0C, $c_{resp,rt}$ is the maintenance respiration coefficient for the root at 25^0C, $c_{Q10,resp}$ is the Q10 factor for maintenance respiration which has a value of 2. c_τ denotes ratio of root dry weight as a function of total dry weight.

1.5. Integrating spectral impact and photoinhibition in lettuce growth model

Experimental results are utilized to relate changes in specific leaf area, maximum rate of photosynthesis and root to shoot ratio to change in spectra of incident sunlight in the PAR region. The spectral change is analyzed based on differences in % blue (400-500 nm) and red (600-700 nm): blue (400-500 nm) (R:B) ratio. Wang et al. observed that different R:B ratios significantly affected photosynthesis as a function of light intensity[6] as shown in **Figure S2(A)**. The value of light saturated photosynthesis increases with the increase in the amount of blue on the PAR spectra up to a R:B value of 1. The authors see a slight reduction in light saturated photosynthesis rate during the absence of the red part of the spectra.

While R:B ratio impacts photosynthesis, the % blue in the light spectra has been shown to impact biomass partitioning to root and shoot. Increase in % blue is shown to improve root development at the cost of biomass partitioning to the shoot[8] as shown in **Figure S2(B)**. Root to shoot ratio impact both respiration loss and in turn total plant dry mass. % blue also impacts the specific leaf area (SLA) which denotes the fraction of increase in leaf area as a ratio of increase in biomass. This is indicated by the work done by Cope et al.[9] SLA as a function of % blue is shown in **Figure S2(C)**. The curve indicates high leaf area expansion at low % blue content and reduces rapidly

before becoming constant at around 20 percent blue. The high SLA is attributed to shade avoidance responses at low % blue.

Lettuce being a low light requiring crop oftentimes adapts its leaf area based on available light intensity. The work done by Fu et al., indicates that a DLI of 20-30 moles m^{-2} day^{-1} is optimal for the growth of lettuce.[10] Work done by Ravishankar et al, indicates that lettuce grown under ST-OSC filters with a DLI of about 13 -17 moles m^{-2} day^{-1} has similar yield to that of a reference lettuce grown under almost twice the amount of light received under the filters.[11] This was because lettuce adapted to changes in light intensity by changing its leaf area expansion. At the same time, at extremely high and low light intensities, lettuce loses part of its efficiency to utilize light absorbed to drive photosynthesis defined by quantum yield of photosystem II (ΦPSII).[10] The experimentally obtained results is utilized to model SLA for various light intensities and this is again shown **Figure S2(C)**.

2. Description of Tomato growth model

The tomato crop is divided into components of leaves, stem, fruit, and roots for the purpose of modelling. Leaves and stem are lumped together as vegetative tissue and total weight is maintained in the model. The structure of the model is based on the work done by Jones et al.[12] Photosynthesis and respiration rates are computed on an hourly basis and integrated to obtain daily increment and total and fruit dry mass. The model relates leaf area expansion, dry matter partitioning to fruit and vegetative tissue were developed for daily calculations of leaf area expansion, dry matter partitioning to fruit and vegetative tissue. Important aspects of the model are discussed here.

2.1. Node development (N)

Nodes are the points on a stem where the buds, leaves and branching twigs originate for a tomato plant.[13] The rate of node development was modeled as a maximum rate of node appearance rate per day multiplied by a function that reduces vegetative development under non-optimal temperatures on an hourly basis during each day. Rate of change of node development is given by,

$$\frac{dN}{dt} = N_m f_N(temp_{plant}),$$ (28)

where N_m is the maximum rate of node appearance (at optimal temperatures), $f_N(temp_{plant})$ is the function to modify node development rate as a function of hourly temperature.

2.2. Leaf Area Index (LAI)

For tomatoes, the LAI is expressed as a function of node position on the plant. The impact of LAI due to temperature variation is accounted through the corresponding impact of temperature on node development is given by,

$$\frac{d(LAI)}{dt} = \frac{d(LAI)}{dN} \cdot \frac{dN}{dt},$$

(29)

where LAI is related to N by the following equation,

$$LAI = \rho \left(\frac{\delta}{\beta}\right) \ln\{1 + e^{[\beta(N-N_b)]}\},$$

where ρ is the plant density, δ is the maximum leaf area expansion per node, β is the normalization coefficient in the equation and N_b is a coefficient that projects the linear segment of LAI vs N to the horizontal axis,

By substituting the expression for $\frac{d(LAI)}{dN}$ and introducing equation (28) for $\frac{dN}{dt}$, we get two case scenarios for the rate of change of LAI in comparison to a maximum LAI parameter. Maximum LAI is the point beyond which there is no further increase in LAI. When LAI is less than maximum LAI, the rate of change of LAI is given by,

$$\frac{d(LAI)}{dt} = \rho\delta\lambda(temp_{plant}) \frac{e^{[\beta(N-N_b)]}}{1+e^{[\beta(N-N_b)]}} \frac{dN}{dt},$$

(30)

where $\lambda(temp_{plant})$ is a temperature function that reduces the rate of leaf area expansion.

Beyond the maximum LAI point, it is assumed that the leaves will be pruned or senesced to maintain a constant maximum LAI thereafter.[12] Hence the rate of change of LAI becomes 0.

2.3. Fruit Dry Matter (W_F)

Fruit dry weight was included by introducing a coefficient for the fraction of above-ground biomass growth partitioned daily to fruit after its development begins. This is assumed to begin at a specified developmental time or node position on the plant when the first fruit on the plant is above 10 mm in diameter.[12] Fruit weight is calculated using the net aboveground biomass growth rate given by:

$$GR_{net} = E(P_g - R_m)[1 - f_R(N)] ,$$

(31)

Where E is the growth efficiency which is defined as the ratio of biomass to photosynthate available for growth, $f_R(N)$ is the fraction of daily growth partitioned to roots, P_g is the daily integral of gross photosynthesis given by[14],

$$P_g = \frac{D\ P_{g,max}\ temp\text{-}factor}{PEEC_{tomato}} \frac{log\left(\left(\left((1-m)\ P_{g,max}\right)+\left(Q_e\ PEEC_{tomato}\ DLI\right)\right)\right)}{\left(\left((1-m)P_{g,max}\right)+\left(\left(Q_e\ PEEC_{tomato}\ DLI\right)\ e^{(-PEEC_{tomato}\ LAI)}\right)\right)}, \tag{32}$$

where D is the conversion factor of CO_2 from µmol CO_2 m^{-2} s^{-1} to g CO_2 m^{-2} day^{-1}, $P_{g,max}$ is the light saturated leaf CO_2 assimilation rate, temp-factor is the factor accounting for the effect of ambient temperature on gross assimilation, $PEEC_{tomato}$ is the plant effective extinction coefficient for tomato, m is the leaf light transmission coefficient, Q_e is the leaf quantum efficiency, DLI is the daily light integral in the photosynthetically active radiation region incident on plants.

R_m denotes the daily integral of maintenance respiration[15] given by,

$$R_m = \int Q_{10}^{\frac{temp_{plant}-20}{10}} \cdot (r_m \cdot (W - W_F) + (r_f \cdot W_F)) \cdot dt, \tag{33}$$

where r_m and r_f are the respiration coefficients, (W-W_F) is the growing mass and W_F is the fruit mass.

Partitioning of aboveground growth to fruit each day beings at node position N_{FF} and increases asymptotically to a maximum partitioning using the following equation,

$$\frac{dW_F}{dt} = GR_{net} \cdot \alpha_F \cdot f_F \cdot \left[1 - e^{-v(N-N_{FF})}\right] \cdot g(temp_{daytime,plant}) \text{ if } N>N_{FF}, \tag{34}$$

where α_F is the maximum partitioning of new growth to fruit, f_F is the parameter that modifies partitioning to fruits, v denotes the transition coefficient between vegetative and full fruit growth, $g(temp_{daytime,plant})$ is the function that reduces growth due to high daytime temperature if it is higher than a critical temperature given by,

$$g(temp_{daytime,plant}) = 1 - 0.154 \cdot (temp_{daytime,plant} - temp_{crit}) \text{ if } temp_{daytime,plant}>temp_{crit}, \tag{35}$$

where $temp_{daytime,plant}$ is the daily average temperature of the plant during day time, $temp_{crit}$ is the defined critical temperature, 0.154 is the slope computed based on experiments.[12]

2.4. Aboveground biomass accumulation (W)

Biomass accumulation is the result of photosynthesis, respiration and tissue conversion processes. The aboveground biomass accumulation is given by,

$$\frac{dW}{dt} = GR_{net} - p_1 \cdot \rho \cdot \left(\frac{dN}{dt}\right), \tag{36}$$

where p_1 is the dry matter of leaves removed per plant per node development after LAI_{max} is reached and a constant value thereafter. Under some conditions, the fruit dry matter growth may be very low due to high temperatures and there will be excess carbohydrate available. The tomato

model does not explicitly include sink strength calculations. Therefore, we assume that there is a maximum rate of vegetative growth per node and that the rate of change of biomass accumulation may be restricted by this limit if fruit growth is limited given by,

$$\left(\frac{dW}{dt}\right) max = \frac{dW_F}{dt} + (V_{max} - p_1).\rho\frac{dN}{dt}. \tag{37}$$

Total above ground dry matter growth is the minimum of equation (36) and (37) and is given by,

$$\frac{dW}{dt} = min\left(\frac{dW}{dt}, \left(\frac{dW}{dt}\right) max\right). \tag{38}$$

3. Description of Koppen-Geiger climate categories

Tropical climates are categorized by constant high temperatures and high relative humidity exceeding 75 %.[16] Based on annual precipitation received, these climates are further sub-categorized into rainforest, monsoon, and savanna climates. Arid climates are characterized by low annual precipitation and the various regions are classified into arid and semi-arid hot/cold conditions accordingly. Hot arid and semi-arid climates have an average annual temperature above 18 °C (64 °F). Cold arid and semi-arid climates have winter temperatures that fall below -3 °C (27 °F). Temperate climates have an average temperature above -3 °C (27 °F) in their coldest month but below 18 °C (64 °F) fall under the broad category of temperate climates. This climate is further divided into sub-categories based on amount of precipitation received and degree of summer heat into subtropics, mediterranean, highland, highland-oceanic and subpolar oceanic climates. Snow climates has an average temperature of above 10 °C (50 °F) in the warmest months and below -3 °C (27 °F) in the coldest month. Snow climates are sub-categorized into humid and mediterranean climates that range from hot summer to extremely cold subarctic climate. While some of the hot summer climates have temperature exceeding 22 °C (72 °F), the subarctic climates have winter temperatures as low as -38 °C (-36 °F). Finally, the polar climates are defined by the warmest temperature of any month not exceeding 10 °C (50 °F). This is subcategorized into tundra and icecap climates with the latter having no months in the year where temperature exceeds 0 °C (32 °F).
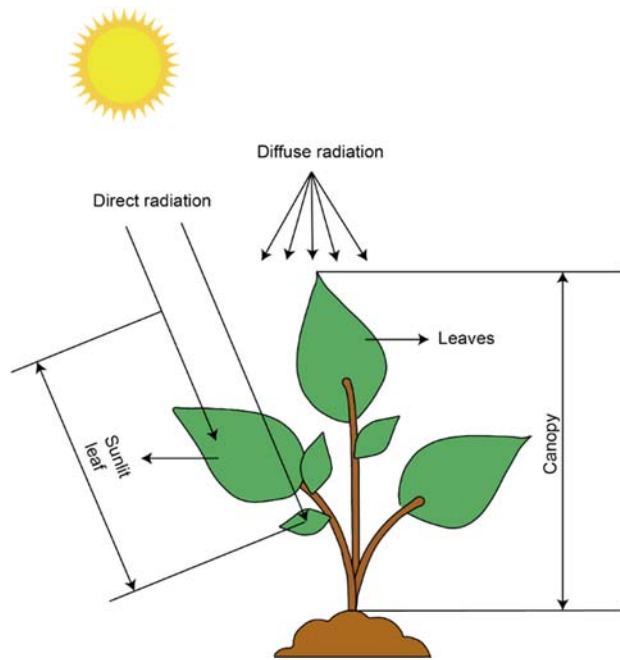
Figure S1. Depiction of absorption of direct and diffuse sunlight over plant canopy.
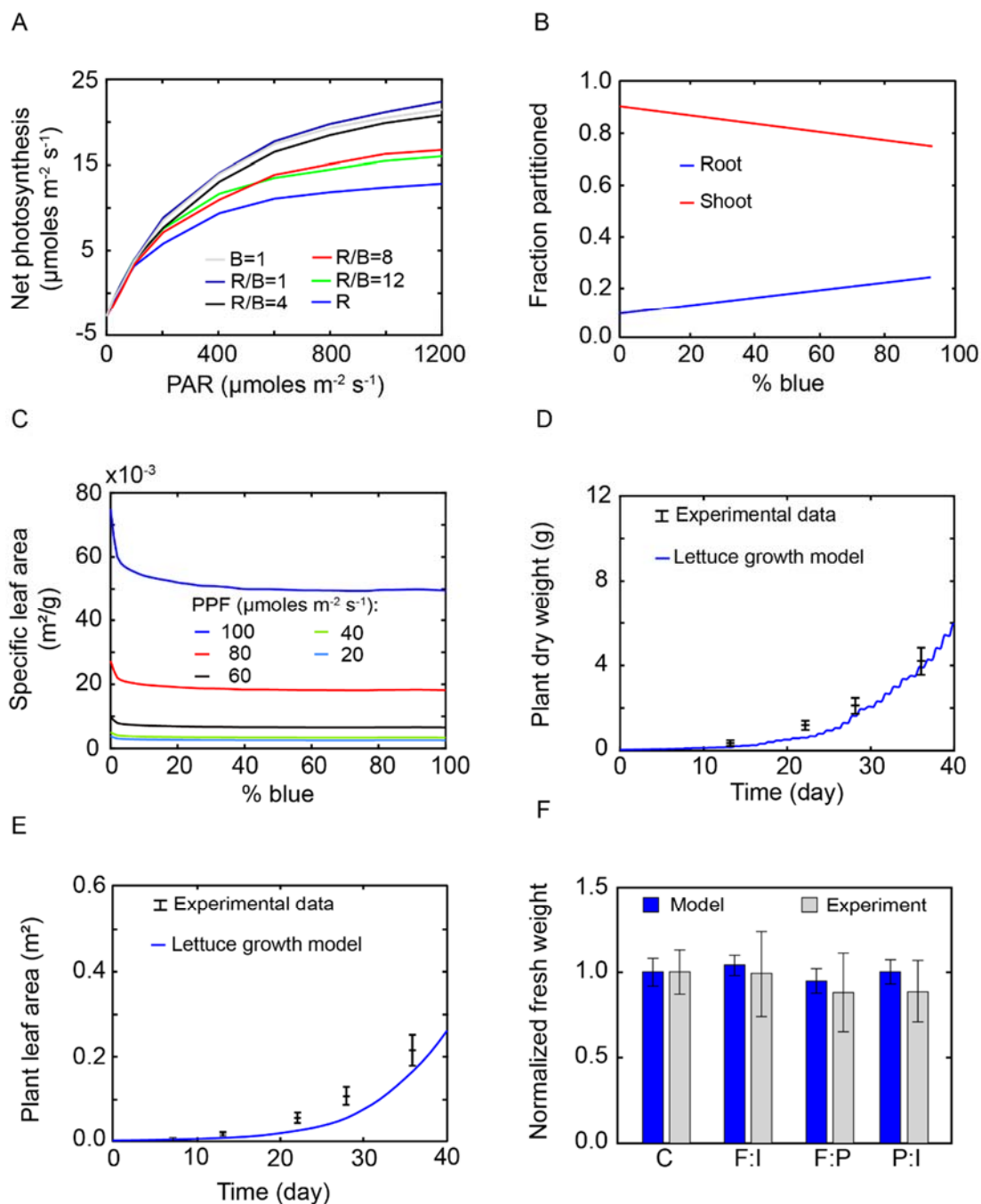
Figure S2. (A) Net photosynthesis as a function of R:B ratio and PAR light intensity.[6] (B) Fraction partitioned to root and shoot as a function of % blue.[8] (C) Change in specific leaf area for lettuce as a function of % blue.[17,18] Validation of (D) dry weight and (E) leaf area obtained from the lettuce growth model with corresponding experimental data in Henten et al.[2] (F) Validation of lettuce growth model with experimental lettuce growth[11] under a control (C) and three organic solar cell filters namely – FTAZ:IT-M (F:I), FTAZ:PCBM (F:P) and PTB7-Th:IEICO-4F (P:I).
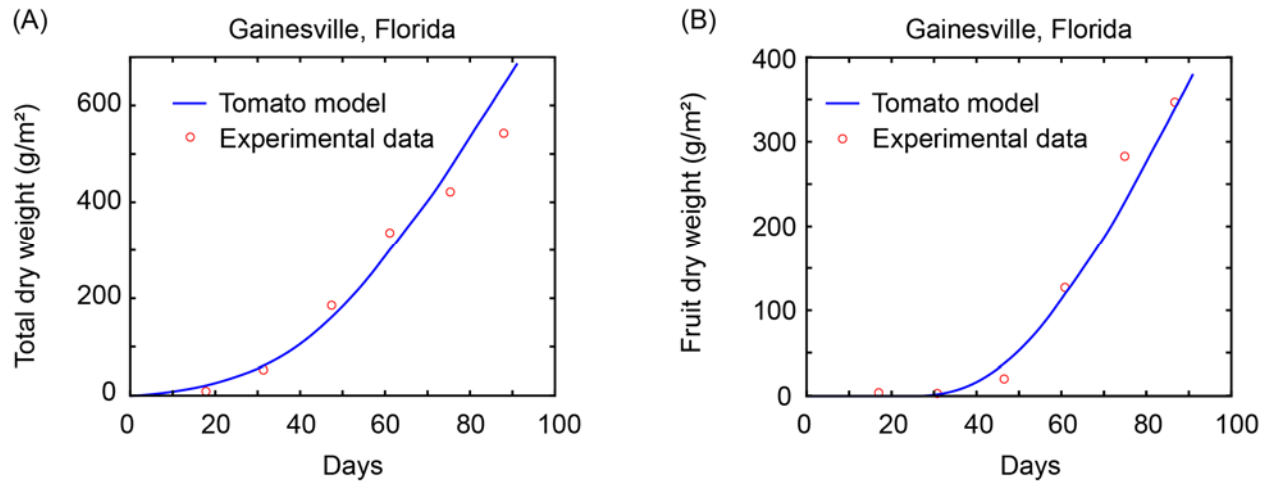
13

Figure S3. (A) Validation of tomato's dry weight and (B) mature fruit weight obtained from the tomato growth model with corresponding experimental data.
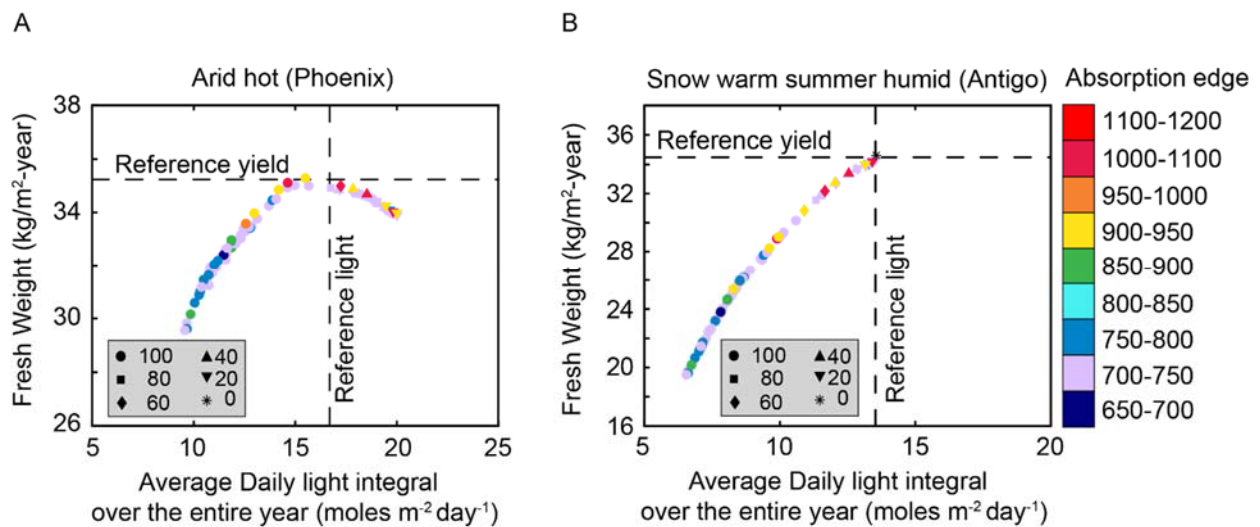

Figure S4. Fresh weight of lettuce as a function of average day light integral in (A) arid hot (Phoenix) and (B) Snow warm summer humid (Antigo). This is for the various solar cell systems and coverages considered relative to the conventional system.
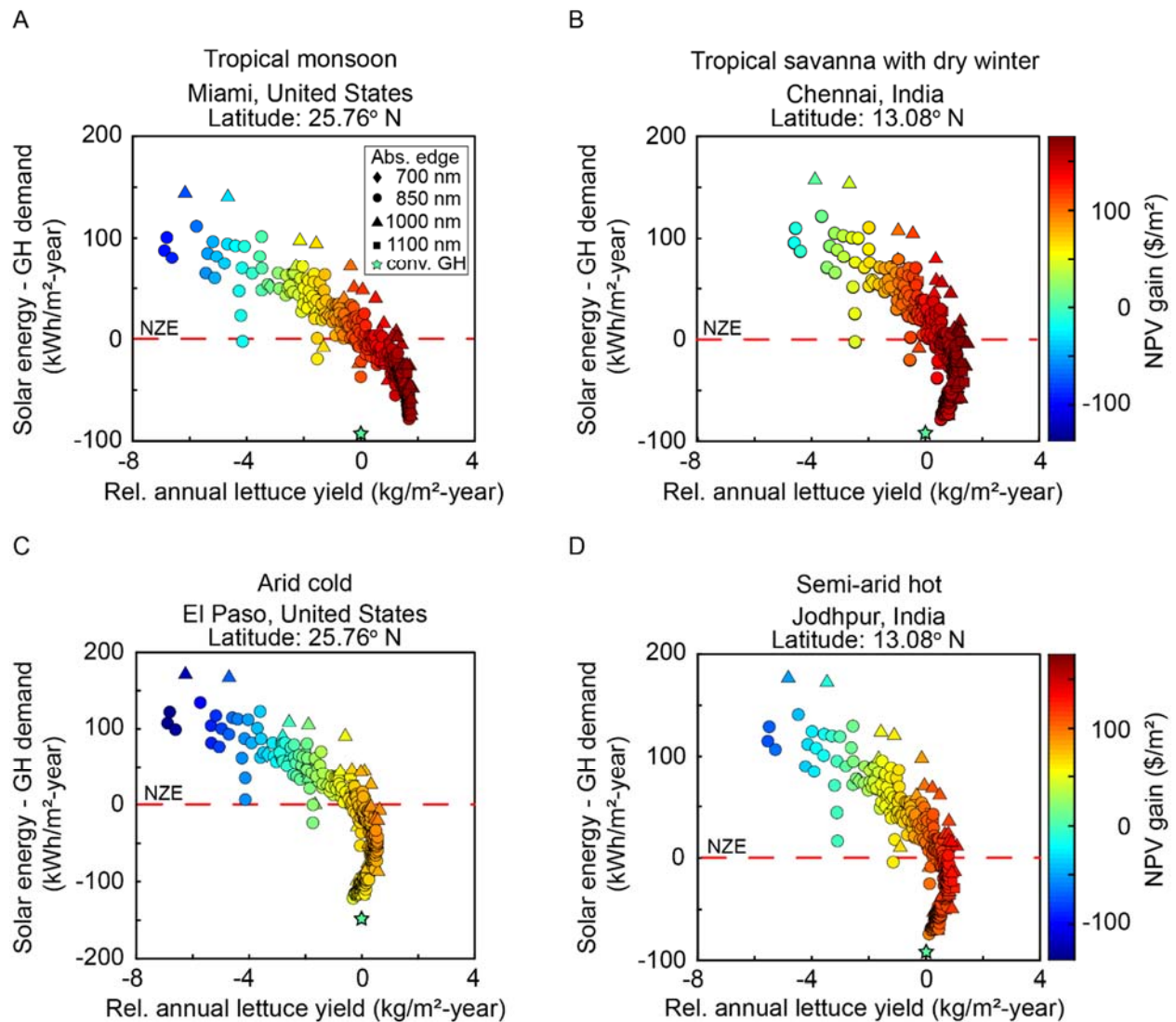
Figure S5. "Base case" NPV as a function of relative annual lettuce yield and difference between solar energy and greenhouse demand in (A) tropical monsoon (Miami), (B) tropical savanna – dry winter (Chennai), (C) dry cold arid (El paso) and (D) dry hot semi-arid (Jodhpur) climates. Lettuce yield and NPV gain is measured relative to the conventional greenhouse system for each climate. NPV gain is normalized to the greenhouse floor area.

Figure S6. "Base case" NPV as a function of relative annual lettuce yield and difference between solar energy and greenhouse demand in (A) dry cold semi-arid (Denver), (B) temperate humid subtropical (Raleigh), (C) temperate subpolar oceanic (Unalaska) and (D) temperate monsoon humid subtropical (Guwahati) climates. Lettuce yield and NPV gain is measured relative to the conventional greenhouse system for each climate. NPV gain is normalized to the greenhouse floor area.

Figure S7. "Base case" NPV as a function of relative annual lettuce yield and difference between solar energy and greenhouse demand in (A) temperate warm summer mediterranean (Seattle), (B) snow hot summer humid (Chicago), (C) snow warm summer humid (Antigo) and (D) snow subarctic (Leadville) climates. Lettuce yield and NPV gain is measured relative to the conventional greenhouse system for each climate. NPV gain is normalized to the greenhouse floor area.
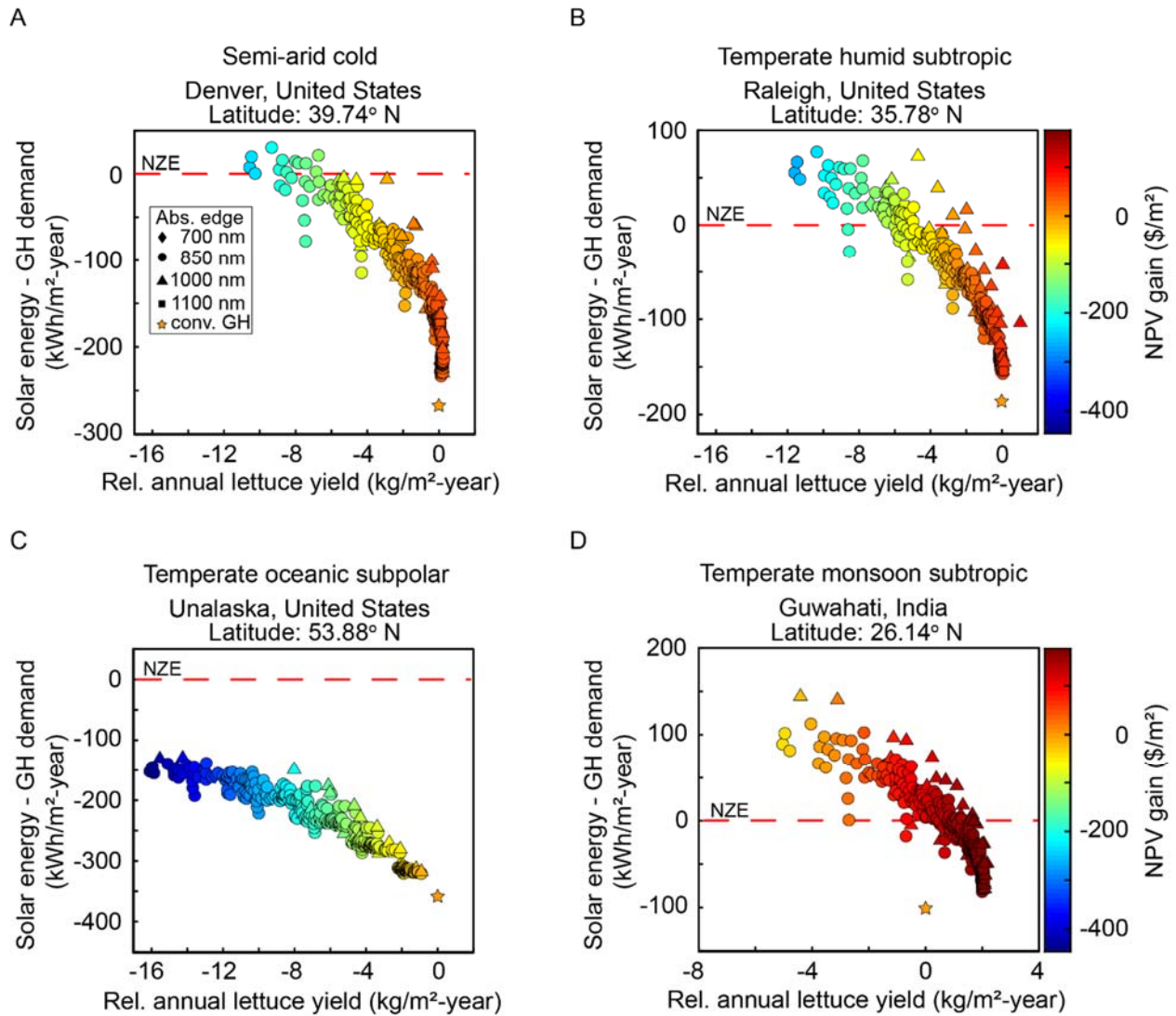
Figure S8. "Base case" NPV as a function of relative annual lettuce yield and difference between solar energy and greenhouse demand in (A) snow monsoon hot summer humid (Pyongyang), (B) snow monsoon warm summer humid (Calgary), (C) snow monsoon subarctic (Yushu City) and (D) snow warm summer humid mediterranean (South lake tahoe) climates. Lettuce yield and NPV gain is measured relative to the conventional greenhouse system for each climate. NPV gain is normalized to the greenhouse floor area.
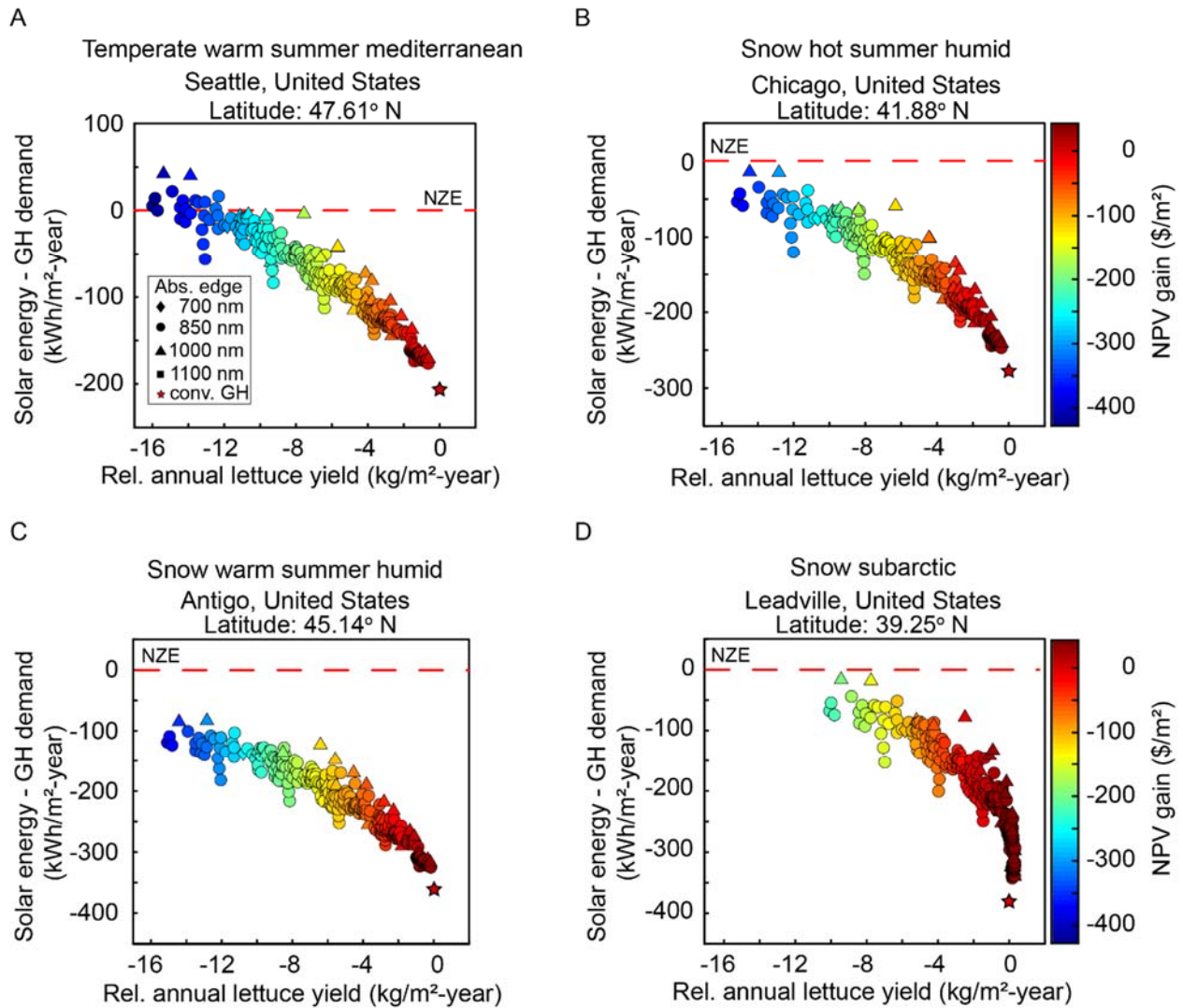
.

Figure S9. "Base case" NPV as a function of relative annual tomato fruit yield and difference between solar energy generated and greenhouse demand in (A) tropical monsoon (Miami), (B) tropical savanna – dry winter (Chennai), (C) dry cold arid (El Paso) and (D) dry hot semi-arid (Jodhpur) climates. Annual fruit yield and NPV gain is measured relative to the conventional greenhouse system for each climate. NPV gain is normalized to the greenhouse floor area.
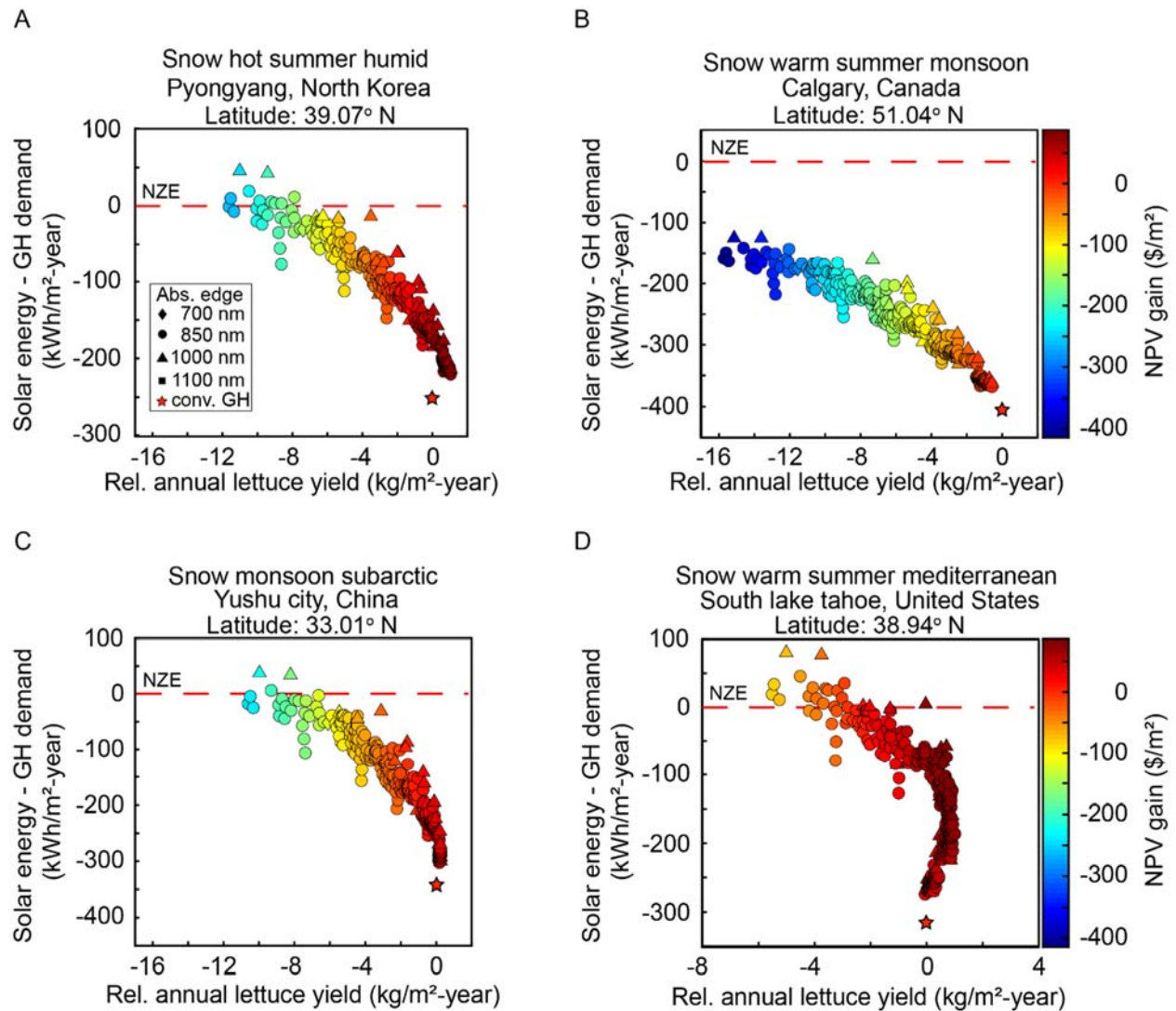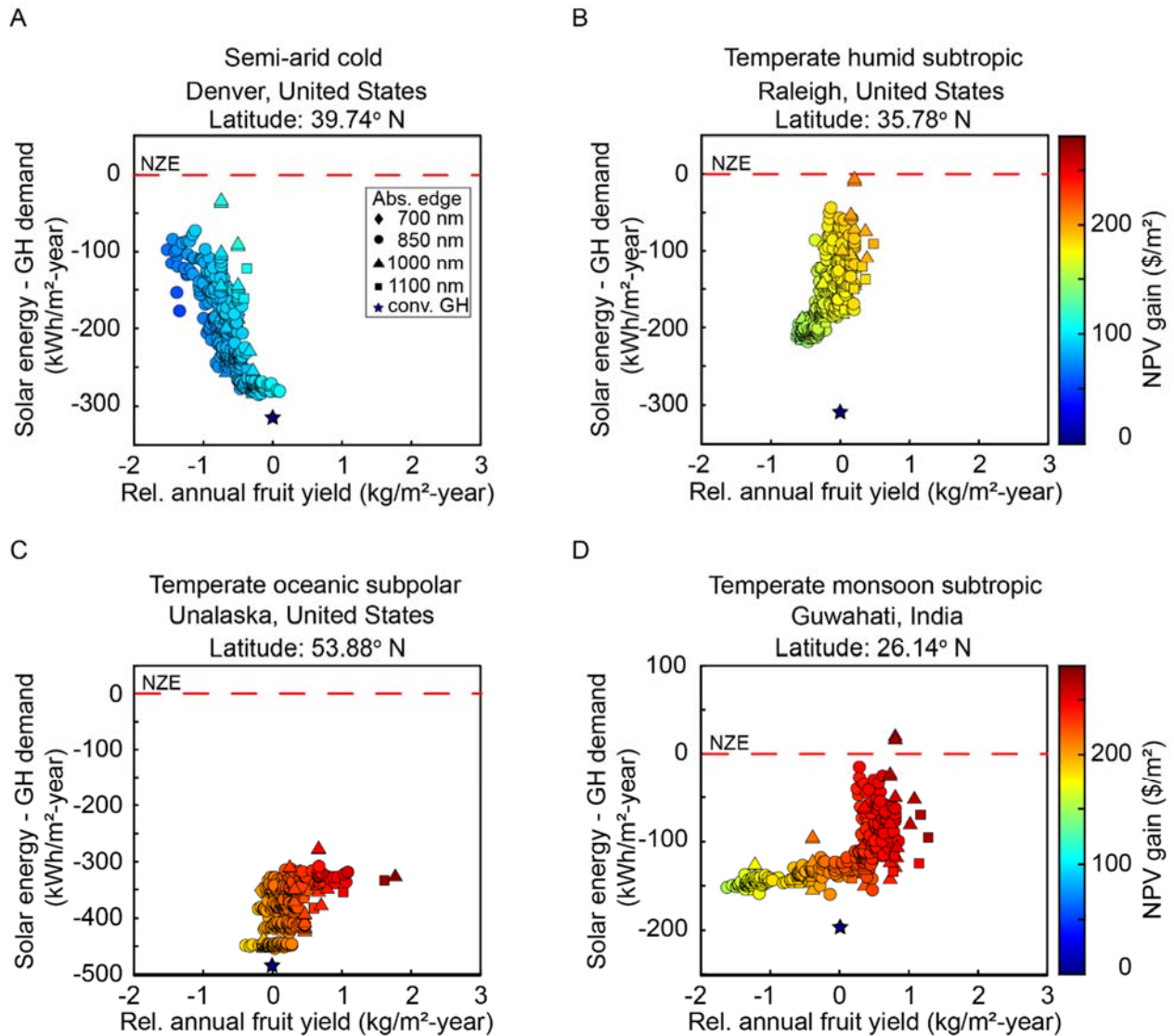
Figure S10. "Base case" NPV as a function of relative annual tomato fruit yield and difference between solar energy generated and greenhouse demand in (A) dry cold semi-arid (Denver), (B) temperate humid subtropical (Raleigh), (C) temperate subpolar oceanic (Unalaska) and (D) temperate monsoon humid subtropical (Guwahati) climates. Annual fruit yield and NPV gain is measured relative to the conventional greenhouse system for each climate. NPV gain is normalized to the greenhouse floor area.
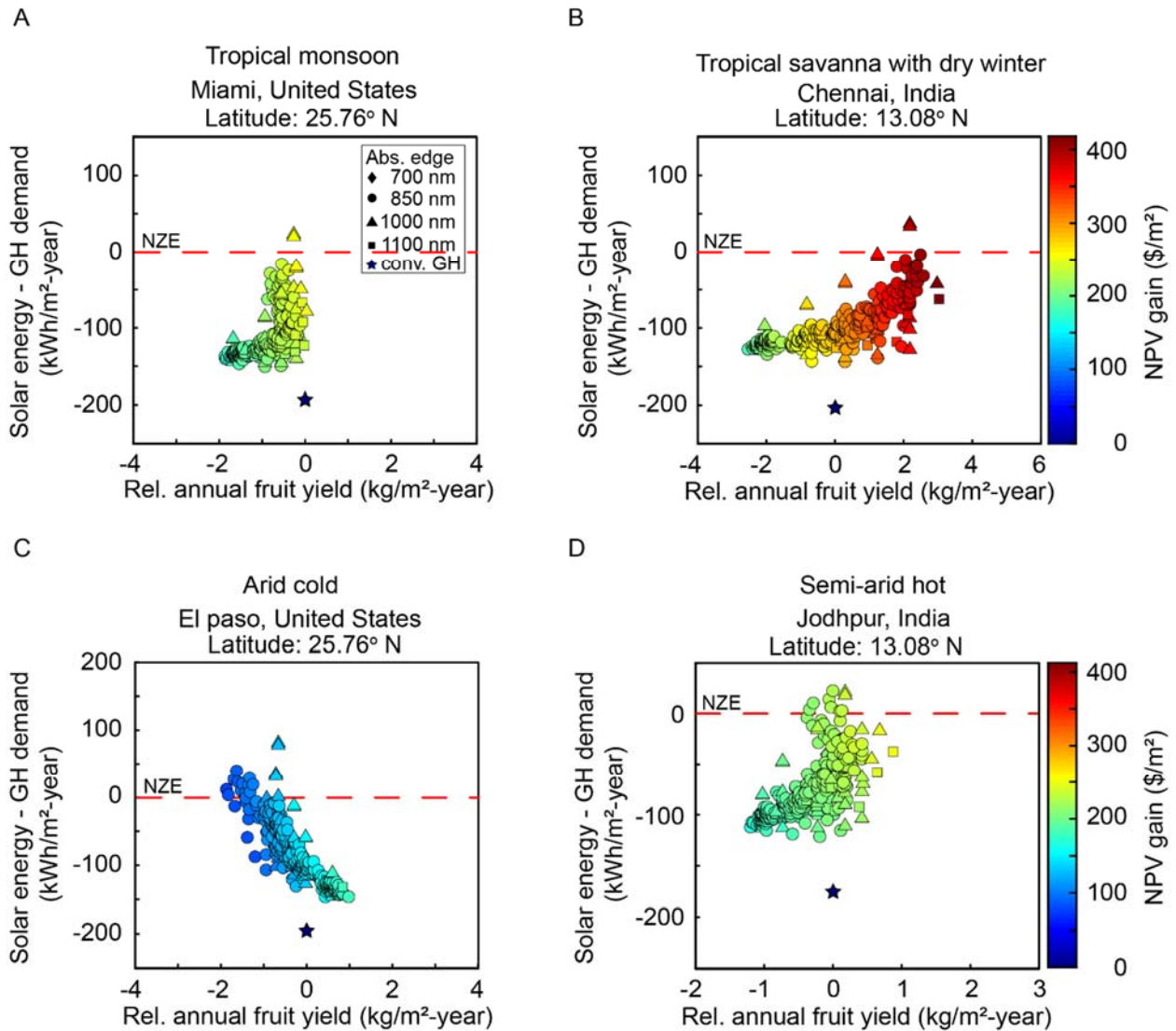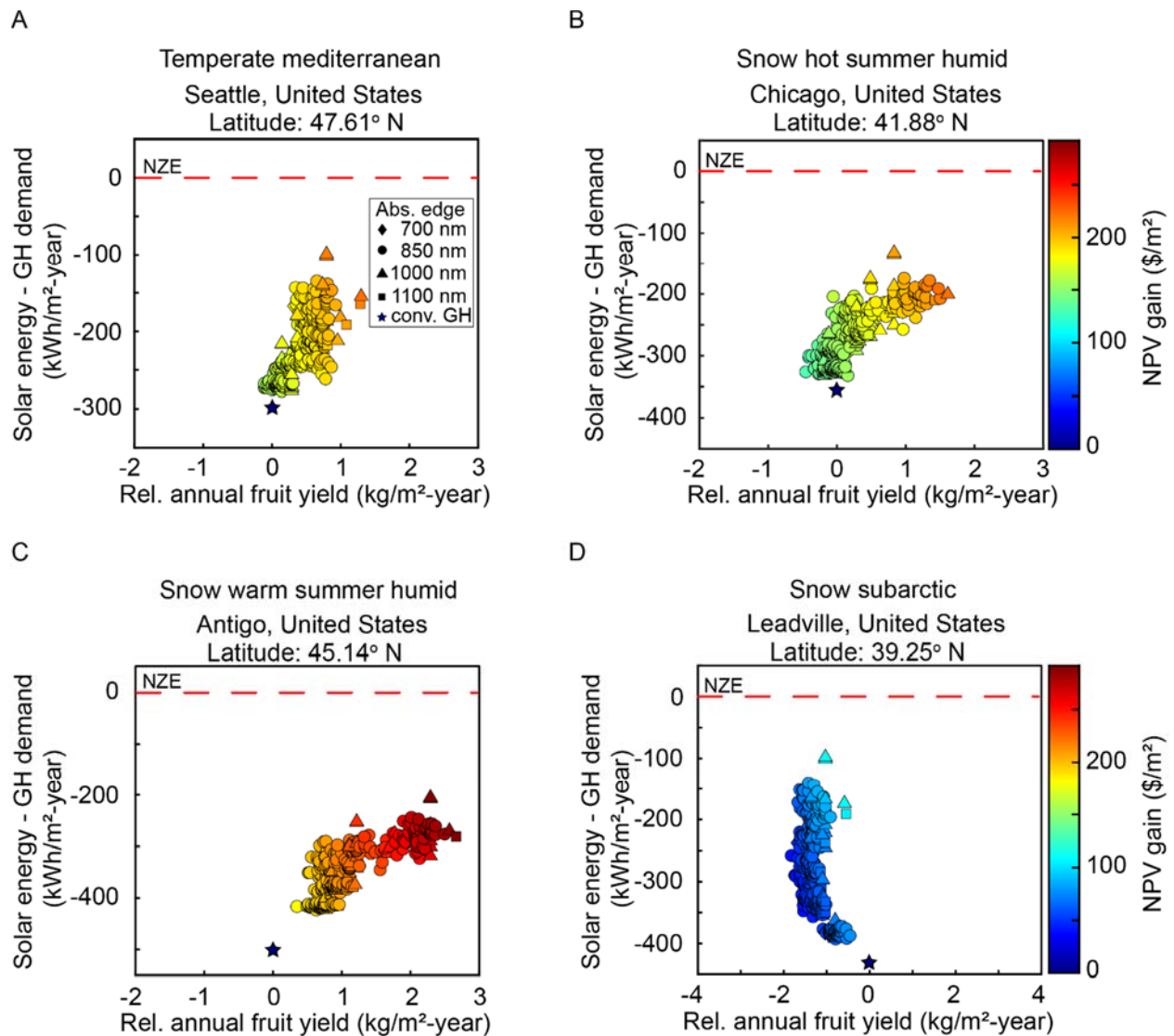
Figure S11. "Base case" NPV as a function of relative annual tomato fruit yield and difference between solar energy generated and greenhouse demand in (A) temperate warm summer mediterranean (Seattle), (B) snow hot summer humid (Chicago), (C) snow warm summer humid (Antigo) and (D) snow subarctic (Leadville) climates. Annual fruit yield and NPV gain is measured relative to the conventional greenhouse system for each climate. NPV gain is normalized to the greenhouse floor area.

Figure S12. "Base case" NPV as a function of relative annual tomato fruit yield and difference between solar energy generated and greenhouse demand in (A) snow monsoon hot summer humid (Pyongyang), (B) snow monsoon warm summer humid (Calgary), (C) snow monsoon subarctic (Yushu city) and (D) snow warm summer humid mediterranean (South lake tahoe) climates. Annual fruit yield and NPV gain is measured relative to the conventional greenhouse system for each climate. NPV gain is normalized to the greenhouse floor area.
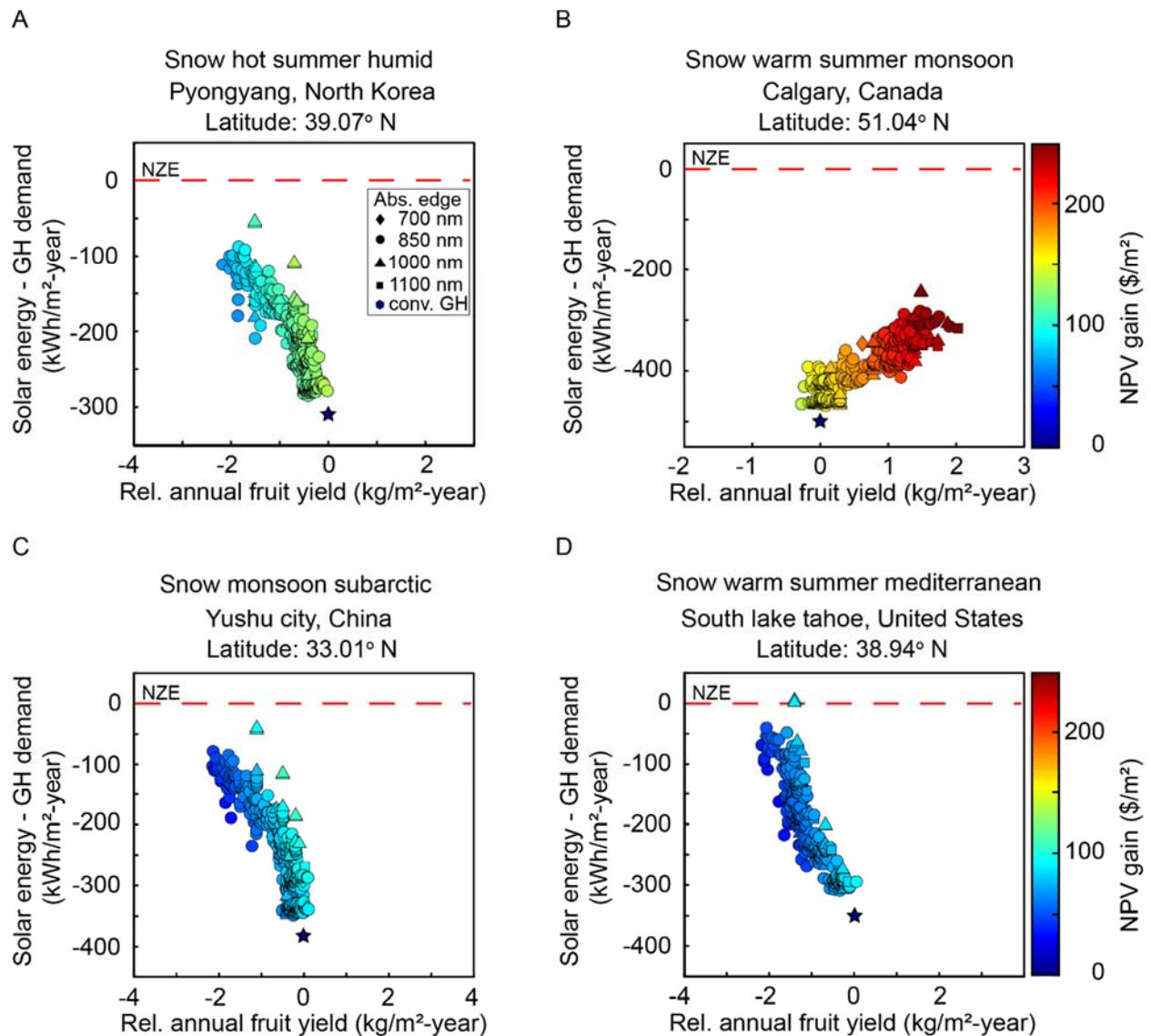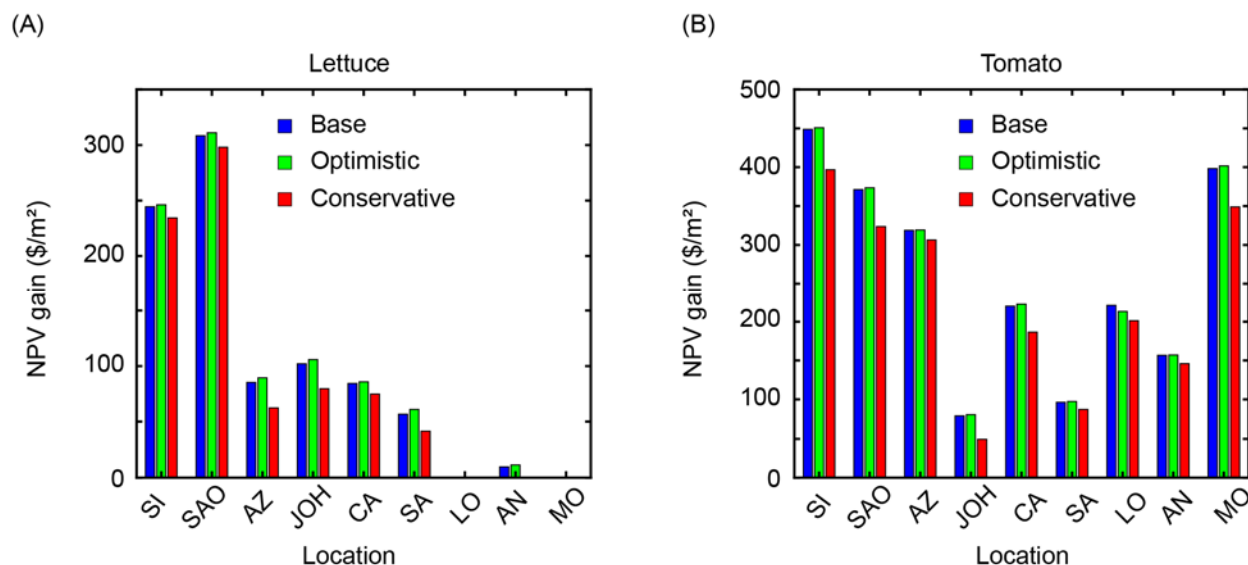
Figure S13. The relative gain in "base case", "optimistic" and "conservative" NPV per unit greenhouse floor area with roof integrated OSCs for (A) lettuce and (B) tomato. The locations modelled are Singapore (SI), Sao Luis (SAO), Phoenix (AZ), Johannesburg (JOH), Sacramento (CA), Salt Lake City (SA), London (LO), Anchorage (AN) and Mount Washington (MO).

TABLE S1. Day light integral of popular greenhouse plants.

Plants	Recommended DLI range for normal plant growth (moles m^{-2} day^{-1})	Associated country for greenhouse production[a]	Reference
Lettuce	13-17	China, Japan	Ravishankar et al (2021)[11]
Tomato	12-30	China, Spain, South Korea, Turkey, Italy, Morocco, Poland, Hungary	Fisher and Runkle (2004)[88]
Cucumber	12-30	China, Spain, South Korea, Turkey, Italy, France, France, Poland	Fisher and Runkle (2004)[88]
Sweet pepper	12-30	China, South Korea	Fisher and Runkle (2004)[88]
Zucchini	10-30	Italy	Rouphael and Colla (2004)[89]
Melon	12-30	South Korea, Turkey, Italy, Japan	Murakami et al (2017)[90]
Cabbage	10-15	China	Mizuno et al (2011)[91]

Asparagus	13-19	China, Japan, Italy, France	Cossu et al (2020)[92]
Radish	10-15	China, Italy	Fisher and Runkle (2004)[88]
Spinach	13-19	China, Japan, Turkey	Fisher and Runkle (2004)[88]
Rocket	13-19	Italy, Morocco, China	Fisher and Runkle (2004)[88]
Bok Choy	10-15	China	Mizuno et al (2011)[91]
Strawberry	12-19	Morocco	Fisher and Runkle (2004)[88]
Eggplant	12-30	Turkey, Italy, Morocco, Poland	Uzun (2007)[93]
Bell peppers	12-30	China, Spain, Italy, Morocco, Hungary	Fisher and Runkle (2004)[88]
Chilli pepper	12-30	China, South Korea, Poland, Hungary	Fisher and Runkle (2004)[88]

[a] Top ten countries with highest greenhouse area for food production are selected.

TABLE S2. Input parameters used in the lettuce growth model simulation.

Parameter	Value
σ	PAR (400-700 nm): 0.2, IR (700-2000 nm): 0.8
τ_{25} ($\mu g\, CO_2\, m^{-2} s^{-1}$)	40 at 25 °C
c_α	0.68
c_β	0.8
c_τ	0.15
c_Υ	1
Φ_{PSII}	DLI (moles $m^{-2}\, hr^{-1}$) Φ_{PSII} 5 0.56 10 1.00 20 0.93 30 0.89 40 0.75
$c_{gr,max}$	5×10^{-6}
$C_{Q10,\tau}$	2
$c_{Q10,gr}$	1.6

$c_{Q10,resp}$	2
$c_{resp,rt}$ (s^{-1})	1.16×10^{-7}
$c_{resp,sht}$ (s^{-1})	3.47×10^{-7}
g_{bnd}	0.007
g_m	0 at temp$_{plant}$ = 0 ºC 0.005 at temp$_{plant}$ = 25 ºC 0 for temp$_{plant}$ >=39 ºC
Plantingdensity (plants/m^2-ground)	18
r_{bv} (s m^{-1})	20
R_d (µg CO_2 m^{-2} s^{-1})	40
r_s (s m^{-1})	100
spectral-factor	R:B spectral-factor 0 2.15 1 2.25 4 2.06 8 1.68 12 1.60 >12 1.29
wgauss	0.12,0.24,0.28,0.24, 0.12
xgauss	0.047,0.231,0.5,0.769, 0.953
$X_{sdw,initial}$ (g/m^2)	2.025
$X_{nsdw,initial}$ (g/m^2)	0.675

TABLE S3. Input parameters used in the tomato growth model simulation.

Parameter	Value
α_F (day^{-1})	0.80
ρ (plants m^{-2}-ground)	4
δ (m^2-leaf node^{-1})	0.04
β (node^{-1})	0.17
ν (node^{-1})	0.14

$\lambda(temp_{plant})$	$temp_{plant}$ (^oC)	$\lambda(temp_{plant})$
	0	0.00
	9	0.00
	12	0.55
	28	1.00
	50	0.00
CO_2 (ppm)	450	
D	2.60	
E (g-d.w. g^{-1} (CH_2O))	0.70	
f_F	0.95	
$f_R(N)$	Node number	$f_R(N)$
	1	0.20
	12	0.15
	21	0.10
	30	0.07
	50	0.07
	90	0.07
$f_N(temp_{plant})$	$temp_{plant}$	$f_N(temp_{plant})$
	0	0.00
	9	0.00
	12	0.55
	28	1.00
	50	0.00
$PEEC_{tomato}$	0.58	
LAI_{max}	5	
m	0.10	
N_b	16	
N_{FF}	22	
N_m	0.50	
p1 (g-leaf d^{-1})	2	
$P_{g,max}$ ($\mu mol\ CO_2\ m^{-2}\ s^{-1}$)	31	
Q_e ($\mu mol\ CO_2\ \mu mol^{-1}$ photons)	0.07	
Q_{10}	1.40	
r_f (g-CH_2O m^{-2}-ground d^{-1})	0.01	
r_m (g-CH_2O m^{-2}-ground d^{-1})	0.02	
temp-factor	$temp_{plant}$	temp-factor
	0	0.00
	9	0.70
	12	1.00
	15	1.00
	21	1.00

	28	1.00
	35	0.00
	50	0.00
temp$_{crit}$ (^{o}C)	24.40	
V$_{max}$ (g-d.w. node^{-1})	8	

TABLE S4. Donor-Acceptor blends utilized for ST-OSC stack simulation.

Donor:Acceptor[a]	Blend absorption edge[b] (nm)	ST-OSC device PCE (%)	Reference device PCE (%)	ST-OSC – PAR transmittance	Reference
PBDB-T:CPDT-4F	910	7.56	9.47	0.39	Wang et al (2019)[19]
PBDB-T:CPDT-4Cl	910	7.15	9.28	0.39	Wang et al (2019)[19]
D18:Y6	910	14.96	18.22	0.24	Liu et al (2020)[20]
PBDB-T:ITIC	750	10.17	11.50	0.26	Upama et al (2017)[21]
J60:ITIC	750	6.36	8.97	0.36	Bin et al (2016)[22]
J61:ITIC	750	5.89	8.93	0.44	Bin et al (2016)[22]
J71:ITIC	750	9.85	11.40	0.31	Bin et al (2016)[23]
PTzBI-DT:ITIC	750	8.42	9.43	0.33	Fan et al (2017)[24]
PBQ-4F:ITIC	750	10.15	11.34	0.28	Zheng et al (2017)[25]
PBZ-m-CF3:ITIC	750	9.51	10.60	0.22	Li et al (2018)[26]
PBDT-S-2TC:ITIC	750	8.60	10.12	0.34	An et al (2018)[27]
PTzBI:ITIC	750	9.10	10.24	0.30	Fan et al (2017)[28]
PBPD-Th:ITIC	750	8.72	10.80	0.28	Fan et al (2017)[29]
PTBFBz:ITIC	750	6.86	8.33	0.42	Gao et al (2018)[30]
PDCBT:ITIC	750	8.90	10.16	0.33	Qin et al (2016)[31]
asy-PBDBTN:ITIC	750	8.33	10.50	0.37	Li et al (2017)[32]
PTBTz-2:ITIC	750	8.76	10.92	0.37	Bao et al (2017)[33]
HD-PBDT2FT:ITIC	750	6.60	8.70	0.47	Xia et al (2016)[34]
HFQx-T:ITIC	750	7.89	9.40	0.38	Xu et al (2017)[35]
PBTCl:ITIC	750	5.82	7.57	0.46	Wang et al (2017)[36]
PM6:ITIC	750	8.02	9.70	0.38	Wang et al (2017)[37]
PαNBDT-T1:ITIC	750	8.68	9.60	0.25	Liu et al (2017)[38]
PBDTTz-BP:ITIC	750	7.09	8.03	0.25	Wen et al (2018)[39]
PBDTTz-N:ITIC	750	5.42	6.61	0.26	Wen et al (2018)[39]
PBDTS-NQx:ITIC	750	10.82	11.50	0.34	Yu et al (2017)[40]
PBDTSF-FBT:ITIC	750	9.77	11.12	0.34	Zhang et al (2018)[41]
PBDTS-TDZ:ITIC	750	11.57	12.80	0.25	Xu et al (2018)[42]

3MTB:ITIC	750	7.14	8.22	0.38	Hoang et al (2018)[43]
PDRCNBDT:ITIC	750	3.91	5.30	0.61	Liao et al (2018)[44]
PDTP4TFBT:ITIC	750	7.11	9.20	0.40	An et al (2017)[45]
PBDTsThPh-BDD:ITIC	750	9.82	10.51	0.35	Liu et al (2018)[46]
3MTTh:ITIC	750	8.81	9.73	0.21	Park et al (2017)[47]
PTzBI-Ph:ITIC	750	9.53	10.20	0.37	Zhu et al (2018)[48]
PBDB-T:IT-M	740	10.77	11.20	0.24	Li et al (2018)[49]
PBDTBDD:ITIC-M	740	11.24	11.69	0.29	Shi et al (2017)[50]
PDCBT-2F:IT-M	740	5.63	6.60	0.55	Zhang et al (2016)[51]
PBDB-T:IDT-HN	660	8.97	10.22	0.30	Li et al (2018)[52]
PBDB-T:IT-OM-2	740	9.88	11.50	0.35	Li et al (2017)[53]
PBTIBDTT-S:ITIC-F	770	8.63	10.50	0.40	Li et al (2018)[54]
PBDB-T-SF:IT-4F	760	11.92	13.10	0.22	Zhao et al (2017)[55]
PBDBT-F:IT-4F	760	12.21	13.35	0.17	Ye et al (2019)[56]
DRTB-T-C2:IT-4F	760	9.11	11.24	0.33	Yang et al (2018)[57]
PM7:IT-4F	760	11.16	13.10	0.21	Fan et al (2018)[58]
PDTB-EF-T:IT-4F	760	12.91	14.20	0.20	Li et al (2018)[59]
PBDB-TF:IT-2F:IT-4F	760	11.67	13.64	0.25	Gao et al (2018)[60]
PBDB-TF:IDTN	750	9.80	12.20	0.40	Li et al (2017)[61]
PB3T:IT-M	740	11.30	11.90	0.16	Liu et al (2017)[62]
FTAZ:INIC3	780	10.50	11.50	0.23	Dai et al (2017)[63]
PM6:IT-4F	760	10.97	13.92	0.28	Jung et al (2020)[64]
PffBT4T-2DT:SF-PDI$_2$	590	5.15	6.30	0.53	Zhao et al (2015)[65]
PTzBI:N2200	780	6.22	9.16	0.48	Fan et al (2017)[66]
PTB7-Th:ITIC-Th	740	7.95	8.70	0.42	Lin et al (2016)[67]
PDBT-T1:ITIC-Th	740	8.46	9.60	0.36	Lin et al (2018)[67]
PCE10:IDTBR:IDFBR	750	10.90	11.40	0.22	Baran et al (2017)[68]
PTB7-Th:ITIC	740	5.65	6.28	0.49	Lin et al (2015)[69]
PTB7-Th:CTIC-4F	910	10.39	10.90	0.34	Lee et al (2019)[70]
PTB7-Th:CO1-4F	1020	9.12	10.20	0.39	Lee et al (2019)[70]
PTB7-Th:COTIC-4F	1120	5.03	7.30	0.54	Lee et al (2019)[70]
PBDB-T-2F:IT-4Cl	790	9.86	12.39	0.27	Zhang et al (2018)[71]
PM6:Y6	870	15.13	15.70	0.18	Yuan et al (2019)[72]
DPP2T:IEICO-4F	950	6.62	9.13	0.60	Lee et al (2020)[73]
FTAZ:IEICO4F:PCBM	950	5.06	7.78	0.40	Ravishankar et al (2021)[11]
PTB7-Th:IEICO-4F	950	10.48	12.80	0.48	Song et al (2018)[74]
FTAZ:IT-M	740	8.89	10.80	0.31	Ye et al (2018)[75]

a: Source of Reference opaque device data for each active layer blend is indicated in the superscript.
b: Absorption edge is the wavelength of the active layer blend beyond which there is negligible absorption. This is marked by the change in slope in the absorption curve.

TABLE S5. Parameters associated with locations simulated to model ST-OSC greenhouses.

Climate description	Simulated location	Coordinates	Night shade sch.[a]	Day shade sch[b]	Base LCOE[c] ($/kWh)	Optimistic LCOE ($/kWh)	Conservative LCOE[c] ($/kWh)	NPV for conventional greenhouse per unit floor area ($/m^2)
Tropical rainforest	Singapore	1.35 ºN 103.82 ºE	No	Jan-Dec	0.12	0.11	0.21	Lettuce: 285.88 Tomato: -307.44
Tropical monsoon	Miami	25.76 ºN 80.19 ºW	No	Apr-Oct	0.12	0.10	0.20	Lettuce: 474.15 Tomato: -8.69
Tropical savanna with dry winter	Chennai	13.08 ºN 80.27 ºE	No	Jan-Dec	0.11	0.10	0.19	Lettuce: 338.40 Tomato: -321.35
Tropical savanna with dry summer	Sao Luis	2.53 ºS 44.26 ºW	No	Jan-Dec	0.10	0.09	0.18	Lettuce: 393.96 Tomato: -84.91
Arid hot	Phoenix	33.44 ºN 112.07 ºW	Jan-Dec	Apr-Oct	0.10	0.09	0.18	Lettuce: 669.75 Tomato: -18.26
Arid cold	El Paso	31.76 ºN 106.48 ºW	Jan-Mar; Nov-Dec	May-Sep	0.10	0.09	0.18	Lettuce: 745.66 Tomato: -3.96
Semi-arid hot	Jodhpur	26.23 ºN 73.02 ºE	Jan-Feb;Dec	Apr-Nov	0.11	0.10	0.20	Lettuce: 519.48 Tomato: -41.25
Semi-arid cold	Denver	39.73 ºN 104.99 ºW	Jan-May; Sep-Dec	No	0.12	0.11	0.21	Lettuce: 763.22 Tomato: 138.74
Temperate humid subtropic	Raleigh	35.78 ºN 78.64 ºW	Jan-Mar; Nov-Dec	Jun-Aug	0.13	0.11	0.22	Lettuce: 671.35 Tomato: -3.96

Temperate oceanic	London	51.51 ºN 0.12 ºW	All	No	0.20	0.18	0.35	Lettuce: 523.27 Tomato: 153.69
Temperate oceanic subpolar	Unalaska	54.88 ºN 166.53 ºW	All	No	0.22	0.20	0.38	Lettuce: 471.24 Tomato: 234.50
Temperate monsoon subtropic	Guwahati	26.14 ºN 91.73 ºE	Jan	Apr-Oct	0.12	0.11	0.21	Lettuce: 398.32 Tomato: -86.26
Temperate highland	Johannesburg	26.20 ºS 28.04 ºE	Apr-Sep	No	0.10	0.09	0.17	Lettuce: 764.81 Tomato: 217.68
Temperate hot summer mediterranean	Sacramento	38.58 ºN 121.50 ºW	Jan,Dec	Apr-Oct	0.11	0.10	0.19	Lettuce: 695.27 Tomato: -31.19
Temperate warm summer mediterranean	Seattle	47.60 ºN 122.33 ºW	Jan-Jun; Sep-Dec	No	0.16	0.15	0.29	Lettuce: 662.20 Tomato: 102.88
Snow hot summer humid	Chicago	41.87 ºN 87.62 ºW	Jan-May; Oct-Dec	No	0.15	0.13	0.25	Lettuce: 675.38 Tomato: 114.21
Snow warm summer humid	Antigo	45.14 ºN 89.15 ºW	Jan-May; Oct-Dec	No	0.15	0.14	0.27	Lettuce: 627.38 Tomato: 97.60
Snow subarctic	Leadville	39.25 ºN 106.29 ºW	All	No	0.12	0.11	0.21	Lettuce: 748.58 Tomato: 175.04
Snow hot summer humid	Pyongyang	39.03 ºN 125.76 ºE	Jan-May; Oct-Dec	Jul-Aug	0.14	0.12	0.24	Lettuce: 659.00 Tomato: 113.17
Snow warm summer monsoon	Calgary	51.04 ºN 114.07 ºW	All	No	0.16	0.14	0.28	Lettuce: 657.67 Tomato: 143.62

Snow monsoon subarctic	Yushu city	33.01 °N 97.09 °W	All	No	0.12	0.10	0.20	Lettuce: 754.15 Tomato: 153.51
Snow hot summer mediterranean	Salt Lake City	40.76 °N 111.89 °W	Jan-May; Oct-Dec	Jul-Aug	0.12	0.10	0.20	Lettuce: 768.50 Tomato: 167.24
Snow warm summer mediterranean	South Lake Tahoe	38.94 °N 119.97 °W	All	No	0.11	0.09	0.18	Lettuce: 724.59 Tomato: 169.09
Snow subarctic mediterranean	Anchorage	61.21 °N 149.90 °W	All	No	0.13	0.12	0.23	Lettuce: 662.68 Tomato: 249.09
Polar tundra	Mount Washington	44.27 °N 71.30 °W	All	No	0.16	0.14	0.27	Lettuce: 675.55 Tomato: 218.82

[a]Night shading is applicable to both ST-OSC and reference greenhouses.
[b]Day shading is applicable to only reference greenhouses.
[c]Levelized cost of electricity defined as the ratio of current value of all future cost of fabricating and operating ST-OSC over its lifetime and power generation.

TABLE S6. Input parameters for calculating NPV.

Parameter	Base case input	Optimistic input	Conservative input	Reference
Minimum sustainable price of OSC (Manufacturing cost + overhead)[a] ($/W)	0.43	0.43	0.70	Kalowekamo and Baker (2009)[76]
Inverter price ($/W)	0.063	0.063	0.20	Song et al (2017)[77] Sommerfeldt and Madani (2017)[78]
BOS equipment ($/W)	0.24	0.24	0.66	Song et al (2017)[77] Gambhir et al (2016)[79]
Installation labor and associated costs ($/W)	0.20	0.20	0.20	Song et al (2017)[77]
OSC annual operation and maintenance cost ($/W)	0.014	0.014	0.014	Song et al (2017)[77]
DC to AC power ratio	1.40	1.40	1.40	Jones-Albertus et al (2016)[80]

Parameter				Reference
DC to AC conversion loss (%)	30	30	30	Jones-Albertus et al (2016)[80]
Inverter lifetime (years)	20	20	20	Song et al (2017)[77]
Module PCE degradation rate (%/year)	2	1	4	Yang et al (2021)[81]
Initial PCE (%)	8.60	8.60	8.60	Yang et al (2021)[81]
Lifetime of solar cell (years)	10	20	5	Gambhir et al (2016)[79] Hollingsworth et al (2020)[82]
Lifetime of greenhouse structure (years)	30	30	30	Boulard et al (2011)[83]
Discount rate (%)	10	10	10	Hollingsworth et al (2020)[82]
Geometric fill factor	0.85	0.90	0.80	Ravishankar et al (2020)[4]
Large scale efficiency retention (%)	100	100	75	Anderson et al (2020)[84]
Cost of electricity ($/kWh)[b]	0.16	0.16	0.16	The world bank – price of electricity (2019)[85]
Cost of natural gas ($/MMBtu)[b]	7.55	7.55	7.55	U.S. energy information administration (2021)[86]
Cost of land ($/acre)	17000	17000	17000	Hollingsworth et al (2020)[82]
Cost of greenhouse structure ($/m^2)	270	270	270	Hollingsworth et al (2020)[82]
Fertilizer, water, and labor costs ($/m^2)	25	25	25	Hollingsworth et al (2020)[82]
Market value of crop ($/kg)	Lettuce: 3.15 Tomato: 4.4	Lettuce: 3.15 Tomato: 4.4	Lettuce: 3.15 Tomato: 4.4	Ohio state University: Hydroponic crop program: economic budgets (2011)[87]
Planting density (plants/m^2)	Lettuce: 18 Tomato: 4	Lettuce: 18 Tomato: 4	Lettuce: 18 Tomato: 4	Henten (1994)[7] Jones et al (1991)[12]

[a] Manufacturing cost comprises of material, maintenance, utilities, labor, and depreciation costs. At the end of OSC lifetime, its present value is valued at 50 % of the original manufacturing cost. Overhead costs comprise of costs associated with manufacturing operations (e.g., scales, general and administrative (SG&A); research and development (R&D) costs; taxes and interest) and weighted average cost of capital (WACC).

[b] Cost of electricity and natural gas is assumed to increase by 1 % every year.

TABLE S7. Lighting requirements for tomato at various growth stages.

Growth stage	Daily Light Integral (moles m^{-2} day^{-1})
Seedling	13-16
Grafting	5-7
Production	20-50

Table S7. **Nomenclature for parameters in model.**

Lettuce growth model

ϵ – Light use efficiency at very high CO_2 concentration. (µmol CO_2/J)

$\Phi_{d,n}$ – Light flux leaving layer n within the plant canopy in the downward direction. (W/m^2)

$\Phi_{d,n+1}$ – Light flux leaving layer n+1 within the plant canopy in the downward direction. (W/m^2)

Φ_I – Light flux incident through a leaf. (W/m^2)

Φ_T – Light flux transmitted through a leaf. (W/m^2)

$\Phi_{u,n}$ – Light flux leaving layer n within the plant canopy in the upward direction. (W/m^2)

$\Phi_{u,n+1}$ – Light flux leaving layer n+1 within the plant canopy in the upward direction. (W/m^2)

τ – CO_2 compensation point (µmol CO_2 mol^{-1})

τ_{25} – CO_2 compensation at 25^{0}C (µmol CO_2 mol^{-1})

σ – scattering coefficient.

ρ_c – Plant canopy reflection coefficient.

Φ_{PSII} – Quantum yield of PSII

ΔL – Assumed gap between leaves.

c_α – Factor converting CO_2 assimilated into CH_2O.

c_β – Respiratory and synthesis losses of non-structural material due to growth.

c_ϵ – Slope of the linear part of the photosynthesis-light curve. (µmol CO_2/J).

c_τ – Ratio of root dry weight as a function of total dry weight.

C_a – Greenhouse CO2 concentration (µmol CO_2 mol^{-1}).

$c_{resp,sht}$ – Maintenance respiration coefficient for the shoot at 25^{0}C

$c_{resp,rt}$ – Maintenance respiration coefficient for the root at 25^{0}C

$C_{Q10,resp}$ – Q10 factor for maintenance respiration.

$f_{phot,inst}$ – The photosynthetic assimilation at a particular depth. (µmoles CO_2/m^2-s)

$f_{phot,local}$ – Local assimilation rate at a considered depth in a plant canopy. (µmoles CO_2/m^2-s)

$f_{phot,gros}$ – Plant canopy assimilation rate. (μmoles CO_2/m^2-s)

ϵ – Light use efficiency at very high CO_2 concentration. (μmol CO_2/J)

$\Phi_{d,n}$ – Light flux leaving layer n within the plant canopy in the downward direction. (W/m^2)

$\Phi_{d,n+1}$ – Light flux leaving layer n+1 within the plant canopy in the downward direction. (W/m^2)

Φ_I – Light flux incident through a leaf. (W/m^2)

Φ_T – Light flux transmitted through a leaf. (W/m^2)

$\Phi_{u,n}$ – Light flux leaving layer n within the plant canopy in the upward direction. (W/m^2)

$\Phi_{u,n+1}$ – Light flux leaving layer n+1 within the plant canopy in the upward direction. (W/m^2)

τ – CO_2 compensation point (μmol CO_2 mol^{-1})

τ_{25} – CO_2 compensation at 25^0C (μmol CO_2 mol^{-1})

σ – scattering coefficient.

ρ_c – Plant canopy reflection coefficient.

Φ_{PSII} – Quantum yield of PSII

ΔL – Assumed gap between leaves.

c_α – Factor converting CO_2 assimilated into CH_2O.

c_β – Respiratory and synthesis losses of non-structural material due to growth.

c_ϵ – Slope of the linear part of the photosynthesis-light curve. (μmol CO_2/J).

c_τ – Ratio of root dry weight as a function of total dry weight.

C_a – Greenhouse CO2 concentration (μmol CO_2 mol^{-1}).

$c_{resp,sht}$ – Maintenance respiration coefficient for the shoot at 25^0C

$c_{resp,rt}$ – Maintenance respiration coefficient for the root at 25^0C

$C_{Q10,resp}$ – Q10 factor for maintenance respiration.

$f_{phot,inst}$ – The photosynthetic assimilation at a particular depth. (μmoles CO_2/m^2-s)

$f_{phot,local}$ – Local assimilation rate at a considered depth in a plant canopy. (μmoles CO_2/m^2-s)

$f_{phot,gros}$ – Plant canopy assimilation rate. (μmoles CO_2/m^2-s)

F_{mm} – Light saturated maximum rate of photosynthesis. (μmoles CO_2/m^2-s)

F_{nc} – CO_2 saturated rate of photosynthesis. (μmoles CO_2/m^2-s)

$f_{photmax}$ – Maximum rate of photosynthesis. (μmoles CO_2/m^2-s)

$frac_{sun}$ – Fraction of leaves that intercepts direct solar radiation.

f_{resp} – Maintenance respiration loss of plants (g m^{-2} s^{-1})

$I_{abs,par}$ – Absorbed light in the Photosynthetically Active Radiation (PAR) region. (W/m^2)

I_{diff} – Total absorption per plant canopy depth in terms of leaf area for diffuse light. (W/m^2)

$I_{direct,total}$ – Total absorption per plant canopy depth in terms of leaf area for direct light. (W/m^2)

$I_{direct,incident}$ – Incident direct sunlight. (W/m^2)

$I_{sunlit,direct}$ – Total absorption by leaves through direct sunlight. (W/m^2)

$I_{total,diffuse}$ – Total absorption by shaded leaves using diffuse and scattered sunlight. (W/m^2)

$I_{total,direct}$ – Total absorption by leaves exposed to direct sunlight. (W/m^2)

L – Leaf Area Index.

laic – Leaf Area Index at a particular depth in the plant canopy.

$PEEC_{bl}$ – Extinction coefficient of leaves assuming no scattering.

$PEEC_{diff}$ – Extinction coefficient of leaves in spherical configuration exposed to diffuse radiation.

$PEEC_{direct}$ – Extinction coefficient of leaves with incident direct radiation.

$PEEC_{spher,I}$ – Extinction coefficient for leaves in spherical configuration at a given incidence angle.

R – reflectance of light.

r_b – Boundary layer resistance. (s/m)

r_{gr} – Relative growth rate. (s^{-1})

r_m – Mesophyll resistance. (s/m)

r_s – Stomatal resistance. (s/m)

spectral-factor – parameter impacting maximum rate of photosynthesis as a function of spectra.

T – Transmittance of light.

$temp_{plant}$ – Greenhouse plant temperature (°C)

x_{gauss} – Gaussian integration values to compute fraction of leaf area at different depths.

w_{gauss} – Gaussian integration values to compute weight of assimilated photosynthesis at different depths.

X_{nsdw} – Non-structural dry weight (g/m^2)

X_{sdw} – Structural dry weight (g/m^2)

y – A dimensionless function of absorbed sunlight (PAR).

Tomato growth model

α_F – Maximum partitioning of new growth to fruit (fraction d^{-1})

ρ – Plant density (no. plants m^{-2}-ground)

δ – Maximum leaf area expansion per node (m^2-leaf node^{-1})

β – Coefficient (node^{-1})

ν – Transition coefficient between vegetative and full fruit growth (node^{-1})

$\lambda(temp_{plant})$ – Temperature function to reduce rate of leaf area expansion

CO_2 – Available CO_2 (ppm)

D – Conversion factor from μmol CO_2 m^{-2} s^{-1} to g CO_2 m^{-2} day^{-1}

E – Growth efficiency, ratio of biomass to photosynthate available for growth (g-d.w. g^{-1} (CH_2O))

f_F – Parameter to modify partitioning to fruit.

$f_R(N)$ – Fraction of partitioning of biomass to roots as a function of development (node).

$f_N(temp_{plant})$ - Function to modify node development rate as a function of hourly temperature.

LAI_{max} – Maximum Leaf Area Index.

m – Leaf light transmission coefficient .

N_b – Coefficient relating node to leaf area index.

N_{FF} – Nodes per plant when first fruit appears.

N_m – Maximum rate of node appearance at normal temperature.

p1 – Loss of leaf d.w. per node after LAI_{max} is achieved. (g-leaf d^{-1})

$P_{g,max}$ – Light saturated leaf CO_2 assimilation rate (μmol CO_2 m^{-2} s^{-1})

$PEEC_{tomato}$ – Plant effective extinction coefficient for tomato.

Q_e – Leaf Quantum efficiency (μmol CO_2 μmol^{-1} photons)

Q_{10} – Coefficient in maintenance respiration equation

r_f – Respiration coefficient for growing mass (g-CH_2O m^{-2}-ground d^{-1})

r_m - – Respiration coefficient for fruit (g-CH_2O m^{-2}-ground d^{-1})

temp-factor – Factor accounting for the effect of ambient temperature on gross assimilation.

temp$_{crit}$ – Mean daytime temperature above which fruit abortion starts.

V_{max} – Maximum increase in vegetative tissue d.w. growth per node. (g-d.w. node^{-1}).

References

1   J. Goudriaan and H. H. van Laar, *Modelling potential crop growth processes. Textbook with exercises*, Springer Science & Business Media, Dordrecht, Netherlands, 1994.

2   E. J. Van Henten, *Agric. Syst.*, 1994, **45**, 55-72.

3   ASHRAE, *HVAC APPLICATIONS*, Atlanta, USA, 2015.

4   E. Ravishankar, R. E. Booth, C. Saravitz, H. Sederoff, H. W. Ade and B. T. O'Connor, *Joule*, 2020, **4**, 490–506.

5   L. F. M. Marcelis, E. Heuvelink and J. Goudriaan, *Sci. Hortic.*, 1998, **74**, 83-111.

6   J. Wang, W. Lu, Y. Tong and Q. Yang, *Front. Plant Sci.*, 2016, **7**, 1-10.

7   E. J. Van Henten, *Agric. Syst.*, 1994, **45**, 55–72.

8   K. Eskins, *Physiol. Plant.*, 1992, **86**, 439–444.

9   K. R. Cope, M. C. Snowden and B. Bugbee, *Photochem. Photobiol.*, 2014, **90**, 574-584.

10   W. Fu, P. Li and Y. Wu, *Sci. Hortic. (Amsterdam).*, 2012, **135**, 45–51.

11   E. Ravishankar, M. Charles, Y. Xiong, R. Henry, J. Swift, J. Rech, J. Calero, S. Cho, R. E. Booth, T. Kim, A. H. Balzer, Y. Qin, C. Hoi Yi Ho, F. So, N. Stingelin, A. Amassian, C. Saravitz, W. You, H. Ade, H. Sederoff and B. T. O'Connor, *Cell Reports Phys. Sci.*, 2021, **2**, 100381.

12   J. W. Jones, A. Kenig and C. E. Vallejos, *Trans. Am. Soc. Agric. Eng.*, 1999, **42**, 255-265.

13   J. Scholberg, B. L. McNeal, J. W. Jones, K. J. Boote, C. D. Stanley and T. A. Obreza, *Agron. J.*, 2000, **92**, 152–159.

14   B. Acock, D. A. Charles-edwards, D. J. Fitter, D. W. Hand, L. J. Ludwig, J. Warren Wilson and A. C. Withers, *J. Exp. Bot.*, 1978, **29**, 815–827.

15   E. Dayan, H. van Keulen, J. W. Jones, I. Zipori, D. Shmuel and H. Challa, *Agric. Syst.*, 1993, **43**, 165–183.

16   M. C. Peel, B. L. Finlayson and T. A. McMahon, *Hydrol. Earth Syst. Sci.*, 2007, **11**, 1633–1644.

17   K. R. Cope, M. C. Snowden and B. Bugbee, *Photochem. Photobiol.*, 2014, **90**, 574–584.

18   W. Fu, P. Li and Y. Wu, *Sci. Hortic.*, 2012, **135**, 45–51.

19   K. Wang, J. Lv, T. Duan, Z. Li, Q. Yang, J. Fu, W. Meng, T. Xu, Z. Xiao, Z. Kan, K. Sun and S. Lu, *ACS Appl. Mater. Interfaces*, 2019, **11**, 6717–6723.

20   Q. Liu, Y. Jiang, K. Jin, J. Qin, J. Xu, W. Li, J. Xiong, J. Liu, Z. Xiao, K. Sun, S. Yang, X. Zhang and L. Ding, *Sci. Bull.*, 2020, **65**, 272–275.

21   M. B. Upama, M. Wright, M. A. Mahmud, N. K. Elumalai, A. Mahboubi Soufiani, D. Wang, C. Xu and A. Uddin, *Nanoscale*, 2017, **9**, 18788–18797.

22   H. Bin, Z. G. Zhang, L. Gao, S. Chen, L. Zhong, L. Xue, C. Yang and Y. Li, *J. Am. Chem. Soc.*, 2016, **138**, 4657–4664.

23   H. Bin, L. Gao, Z. G. Zhang, Y. Yang, Y. Zhang, C. Zhang, S. Chen, L. Xue, C. Yang, M. Xiao and Y. Li, *Nat. Commun.*, 2016, **7**, 1–11.

24   B. Fan, L. Ying, P. Zhu, F. Pan, F. Liu, J. Chen, F. Huang and Y. Cao, *Adv. Mater.*, 2017, **29**, 1–7.

25   Z. Zheng, O. M. Awartani, B. Gautam, D. Liu, Y. Qin, W. Li, A. Bataller, K. Gundogdu, H. Ade and J. Hou, *Adv. Mater.*, 2017, **29**, 3–8.

26   W. Li, G. Li, X. Guo, Y. Wang, H. Guo, Q. Xu, M. Zhang and Y. Li, *J. Mater. Chem. A*, 2018, **6**, 6551–6558.

27   Y. An, X. Liao, L. Chen, J. Yin, Q. Ai, Q. Xie, B. Huang, F. Liu, A. K. Y. Jen and Y. Chen, *Adv. Funct. Mater.*, 2018, **28**, 1–9.

28   B. Fan, K. Zhang, X. F. Jiang, L. Ying, F. Huang and Y. Cao, *Adv. Mater.*, 2017, **29**, 1606396-1606403.

29   Q. Fan, Z. Xu, X. Guo, X. Meng, W. Li, W. Su, X. Ou, W. Ma, M. Zhang and Y. Li, *Nano Energy*, 2017, **40**, 20–26.

30   Y. Gao, R. Zhu, Z. Wang, F. Guo, Z. Wei, Y. Yang, L. Zhao and Y. Zhang, *ACS Appl. Energy Mater.*, 2018, **1**, 1888–1892.

31   Y. Qin, M. A. Uddin, Y. Chen, B. Jang, K. Zhao, Z. Zheng, R. Yu, T. J. Shin, H. Y. Woo

and J. Hou, *Adv. Mater.*, 2016, **28**, 9416–9422.

32   Y. Li, D. Liu, J. Wang, Z. G. Zhang, Y. Li, Y. Liu, T. Zhu, X. Bao, M. Sun and R. Yang, *Chem. Mater.*, 2017, **29**, 8249–8257.

33   X. Bao, Y. Zhang, J. Wang, D. Zhu, C. Yang, Y. Li, C. Yang, J. Xu and R. Yang, *Chem. Mater.*, 2017, **29**, 6766–6771.

34   D. Xia, Y. Wu, Q. Wang, A. Zhang, C. Li, Y. Lin, F. J. M. Colberts, J. J. Van Franeker, R. A. J. Janssen, X. Zhan, W. Hu, Z. Tang, W. Ma and W. Li, *Macromolecules*, 2016, **49**, 6445–6454.

35   S. Xu, L. Feng, J. Yuan, Z. G. Zhang, Y. Li, H. Peng and Y. Zou, *ACS Appl. Mater. Interfaces*, 2017, **9**, 18816–18825.

36   H. Wang, P. Chao, H. Chen, Z. Mu, W. Chen and F. He, *ACS Energy Lett.*, 2017, **2**, 1971–1977.

37   Y. Wang, Q. Fan, X. Guo, W. Li, B. Guo, W. Su, X. Ou and M. Zhang, *J. Mater. Chem. A*, 2017, **5**, 22180–22185.

38   Z. Liu, D. Liu, K. Zhang, T. Zhu, Y. Zhong, F. Li, Y. Li, M. Sun and R. Yang, *J. Mater. Chem. A*, 2017, **5**, 21650–21657.

39   S. Wen, W. Chen, G. Huang, W. Shen, H. Liu, L. Duan, J. Zhang and R. Yang, *J. Mater. Chem. C*, 2018, **6**, 1753–1758.

40   T. Yu, X. Xu, G. Zhang, J. Wan, Y. Li and Q. Peng, *Adv. Funct. Mater.*, 2017, **27**, 1–11.

41   G. Zhang, X. Xu, Z. Bi, W. Ma, D. Tang, Y. Li and Q. Peng, *Adv. Funct. Mater.*, 2018, **28**, 1–15.

42   X. Xu, T. Yu, Z. Bi, W. Ma, Y. Li and Q. Peng, *Adv. Mater.*, 2018, **30**, 1-8.

43   M. H. Hoang, G. E. Park, D. L. Phan, T. T. Ngo, T. Van Nguyen, S. H. Park, M. J. Cho and D. H. Choi, *J. Polym. Sci. Part A Polym. Chem.*, 2018, **56**, 1528–1535.

44   Z. Liao, Y. Wang, Y. An, Y. Tan, X. Meng, F. Wu, L. Chen and Y. Chen, *Macromol. Rapid Commun.*, 2018, **39**, 1–7.

45   M. An, F. Xie, X. Geng, J. Zhang, J. Jiang, Z. Lei, D. He, Z. Xiao and L. Ding, *Adv. Energy Mater.*, 2017, **7**, 2–7.

46   D. Liu, J. Wang, C. Gu, Y. Li, X. Bao and R. Yang, *Adv. Mater.*, 2018, **30**, 1–9.

47   G. E. Park, S. Choi, S. Y. Park, D. H. Lee, M. J. Cho and D. H. Choi, *Adv. Energy Mater.*, 2017, **7**, 1–10.

48   P. Zhu, B. Fan, X. Du, X. Tang, N. Li, F. Liu, L. Ying, Z. Li, W. Zhong, C. J. Brabec, F. Huang and Y. Cao, *ACS Appl. Mater. Interfaces*, 2018, **10**, 22495–22503.

49   W. Li, J. Cai, Y. Yan, F. Cai, S. Li, R. S. Gurney, D. Liu, J. D. McGettrick, T. M. Watson, Z. Li, A. J. Pearson, D. G. Lidzey, J. Hou and T. Wang, *Sol. RRL*, 2018, **2**, 1–10.

50   Z. Shi, H. Liu, Y. Wang, J. Li, Y. Bai, F. Wang, X. Bian, T. Hayat, A. Alsaedi and Z. Tan, *ACS Appl. Mater. Interfaces*, 2017, **9**, 43871–43879.

51   H. Zhang, S. Li, B. Xu, H. Yao, B. Yang and J. Hou, *J. Mater. Chem. A*, 2016, **4**, 18043–18049.

52   R. Li, G. Liu, R. Xie, Z. Wang, X. Yang, K. An, W. Zhong, X. F. Jiang, L. Ying, F. Huang and Y. Cao, *J. Mater. Chem. C*, 2018, **6**, 7046–7053.

53   S. Li, L. Ye, W. Zhao, S. Zhang, H. Ade and J. Hou, *Adv. Energy Mater.*, 2017, **7**, 1–10.

54   Z. Li, D. Yang, T. Zhang, J. Zhang, X. Zhao and X. Yang, *Small*, 2018, **14**, 1–8.

55   W. Zhao, S. Li, H. Yao, S. Zhang, Y. Zhang, B. Yang and J. Hou, *J. Am. Chem. Soc.*, 2017, **139**, 7148–7151.

56   L. Ye, S. Li, X. Liu, S. Zhang, M. Ghasemi, Y. Xiong, J. Hou and H. Ade, *Joule*, 2019, **3**, 443–458.

57   L. Yang, S. Zhang, C. He, J. Zhang, Y. Yang, J. Zhu, Y. Cui, W. Zhao, H. Zhang, Y. Zhang, Z. Wei and J. Hou, *Chem. Mater.*, 2018, **30**, 2129–2134.

58   Q. Fan, Q. Zhu, Z. Xu, W. Su, J. Chen, J. Wu, X. Guo, W. Ma, M. Zhang and Y. Li, *Nano Energy*, 2018, **48**, 413–420.

59   S. Li, L. Ye, W. Zhao, H. Yan, B. Yang, D. Liu, W. Li, H. Ade and J. Hou, *J. Am. Chem. Soc.*, 2018, **140**, 7159–7167.

60   B. Gao, H. Yao, J. Hou, R. Yu, L. Hong, Y. Xu and J. Hou, *J. Mater. Chem. A*, 2018, **6**, 23644–23649.

61   S. Li, L. Ye, W. Zhao, X. Liu, J. Zhu, H. Ade and J. Hou, *Adv. Mater.*, 2017, **29**, 1–7.

62   D. Liu, B. Yang, B. Jang, B. Xu, S. Zhang, C. He, H. Y. Woo and J. Hou, *Energy Environ. Sci.*, 2017, **10**, 546–551.

63   S. Dai, F. Zhao, Q. Zhang, T. K. Lau, T. Li, K. Liu, Q. Ling, C. Wang, X. Lu, W. You and X. Zhan, *J. Am. Chem. Soc.*, 2017, **139**, 1336–1343.

64   S. Jung, J. Oh, U. J. Yang, S. M. Lee, J. Lee, M. Jeong, Y. Cho, S. Kim, J. M. Baik and C. Yang, *Nano Energy*, 2020, **77**, 105271.

65 J. Zhao, Y. Li, H. Lin, Y. Liu, K. Jiang, C. Mu, T. Ma, J. Y. Lin Lai, H. Hu, D. Yu and H. Yan, *Energy Environ. Sci.*, 2015, **8**, 520–525.

66 B. Fan, L. Ying, Z. Wang, B. He, X. F. Jiang, F. Huang and Y. Cao, *Energy Environ. Sci.*, 2017, **10**, 1243–1251.

67 Y. Lin, F. Zhao, Q. He, L. Huo, Y. Wu, T. C. Parker, W. Ma, Y. Sun, C. Wang, D. Zhu, A. J. Heeger, S. R. Marder and X. Zhan, *J. Am. Chem. Soc.*, 2016, **138**, 4955–4961.

68 D. Baran, R. S. Ashraf, D. A. Hanifi, M. Abdelsamie, N. Gasparini, J. A. Röhr, S. Holliday, A. Wadsworth, S. Lockett, M. Neophytou, C. J. M. Emmott, J. Nelson, C. J. Brabec, A. Amassian, A. Salleo, T. Kirchartz, J. R. Durrant and I. McCulloch, *Nat. Mater.*, 2017, **16**, 363–369.

69 Y. Lin, J. Wang, Z. G. Zhang, H. Bai, Y. Li, D. Zhu and X. Zhan, *Adv. Mater.*,2015, **27**, 1294-1299.

70 J. Lee, S. J. Ko, H. Lee, J. Huang, Z. Zhu, M. Seifrid, J. Vollbrecht, V. V. Brus, A. Karki, H. Wang, K. Cho, T. Q. Nguyen and G. C. Bazan, *ACS Energy Lett.*, 2019, **4**, 1401–1409.

71 Y. Zhang, H. Yao, S. Zhang, Y. Qin, J. Zhang, L. Yang, W. Li, Z. Wei, F. Gao and J. Hou, *Sci. China Chem.*, 2018, **61**, 1328–1337.

72 J. Yuan, Y. Zhang, L. Zhou, G. Zhang, H. L. Yip, T. K. Lau, X. Lu, C. Zhu, H. Peng, P. A. Johnson, M. Leclerc, Y. Cao, J. Ulanski, Y. Li and Y. Zou, *Joule*, 2019, **3**, 1140–1151.

73 J. Lee, H. Cha, H. Yao, J. Hou, Y. H. Suh, S. Jeong, K. Lee and J. R. Durrant, *ACS Appl. Mater. Interfaces*, 2020, **12**, 32764–32770.

74 X. Song, N. Gasparini, L. Ye, H. Yao, J. Hou, H. Ade and D. Baran, *ACS Energy Lett.*, 2018, **3**, 669–676.

75 L. Ye, Y. Xiong, Q. Zhang, S. Li, C. Wang, Z. Jiang, J. Hou, W. You and H. Ade, *Adv. Mater.*, 2018, **30**, 1705485.

76 J. Kalowekamo and E. Baker, *Sol. Energy*, 2009, **83**, 1224–1231.

77 Z. Song, C. L. McElvany, A. B. Phillips, I. Celik, P. W. Krantz, S. C. Watthage, G. K. Liyanage, D. Apul and M. J. Heben, *Energy Environ. Sci.*, 2017, **10**, 1297–1305.

78 N. Sommerfeldt and H. Madani, *Renewable and Sustainable Energy Reviews*, 2017, **74**, 1394-1404.

79 A. Gambhir, P. Sandwell and J. Nelson, *Sol. Energy Mater. Sol. Cells*, 2016, **156**, 49–58.

80 R. Jones-Albertus, D. Feldman, R. Fu, K. Horowitz and M. Woodhouse, *Prog.*

Photovoltaics Res. Appl., 2016, **24**, 1272–1283.

81   W. Yang, W. Wang, Y. Wang, R. Sun, J. Guo, H. Li, M. Shi, J. Guo, Y. Wu, T. Wang, G. Lu, C. J. Brabec, Y. Li and J. Min, *Joule*, 2021, **5**, 1209–1230.

82   J. A. Hollingsworth, E. Ravishankar, B. O'Connor, J. X. Johnson and J. F. DeCarolis, *J. Ind. Ecol.*, 2020, **24**, 234–247.

83   T. Boulard, C. Raeppel, R. Brun, F. Lecompte, F. Hayer and G. Carmassi. *Agron Sustain Dev.*, 2011, **31**, 757–777.

84   T.R. Andersen, F. Zhao, Y. Li, M. Dickinson and H. Chen. *Solar RRL*, 2020, **4**, 1-9.

85   The world bank - price of electricity, https://govdata360.worldbank.org/indicators/h6779690b?country=BRA&indicator=42573 &viz=line_chart&years=2014,2019.

86   EIA, https://www.eia.gov/electricity/data/browser/#/topic/7?agg=2,0,1&geo=g&freq=M .

87   Ohio state university: Hydroponic crop program - economic budgets, https://u.osu.edu/greenhouse/hydroponic-crop-program-economic-budgets/.

88   P. Fisher and E. Runkle, *Lighting up profits: Understanding greenhouse lighting*, Meister Media Worldwide, 2004.

89   Y. Rouphael and G. Colla, *Eur. J. Agron.*, 2005, **23**, 183–194.

90   K. Murakami, N. Fukuoska and S. Noto, *Sci. Hortic.*, 2017, **218**, 1–7.

91   T. Mizuno, W. Amaki and H. Watanabe, *Acta Hortic.*, 2011, **907**, 179–184.

92   M. Cossu, A. Yano, S. Solinas, P. A. Deligios, M. T. Tiloca, A. Cossu and L. Ledda, *Eur. J. Agron.*, 2020, **118**, 126074.

93   S. Uzun, *New Zeal. J. Crop Hortic. Sci.*, 2007, **35**, 51–59.